Qualitative Evaluation of a Flush Air Data System at Transonic Speeds and High Angles of Attack

Terry J. Larson,
Stephen A. Whitmore,
L. J. Ehernberger,
J. Blair Johnson,
and Paul M. Siemers III

NASA

Qualitative Evaluation of a Flush Air Data System at Transonic Speeds and High Angles of Attack

Terry J. Larson,
Stephen A. Whitmore,
L. J. Ehernberger,
and J. Blair Johnson
Ames Research Center
Dryden Flight Research Facility
Edwards, California

Paul M. Siemers III
Langley Research Center
Hampton, Virginia

SUMMARY

Flight tests were performed on an F-14 aircraft to evaluate the use of flush pressure orifices on the nose section for obtaining air data at transonic speeds over a large range of flow angles. This program, conducted at the Dryden Flight Research Facility of NASA Ames Research Center, was part of a flight test and wind-tunnel program to assess the accuracies of such systems for general use on aircraft. It also provided data to validate algorithms developed for the shuttle entry air data system designed at NASA Langley Research Center. Data were obtained for Mach numbers between 0.60 and 1.60, for angles of attack up to 26.0°, and for sideslip angles up to 11.0°. With careful calibration, a flush air data system with all flush orifices can provide accurate air data information over a large range of flow angles. Several orifices on the nose cap were found to be suitable for determination of stagnation pressure. Other orifices on the nose section aft of the nose cap were shown to be suitable for determination of static pressure. Pairs of orifices on the nose cap provided the most sensitive measurements for determining angles of attack and sideslip, although orifices located farther aft on the nose section could also be used.

INTRODUCTION

A wind-tunnel and flight test program was conducted by the Dryden Flight Research Facility of NASA Ames Research Center (Ames-Dryden) to evaluate the use of all flush orifices in a flush air data system (FADS) on aircraft from subsonic to low supersonic speeds (refs. 1 to 5). The work discussed in this report was a continuation of a program designed at NASA Langley Research Center for the shuttle entry air data system (SEADS). It provided data for evaluating algorithms developed from wind-tunnel test results for deriving air data from SEADS measurements (refs. 6 and 7). The SEADS development was initiated to provide data during shuttle entry into the atmosphere, especially when intense aerodynamic heating precludes extending the external side probes into the airstream.

Earlier wind-tunnel and flight tests were conducted for a FADS on a KC-135 airplane and aircraft scale model to provide data for evaluating SEADS algorithms (refs. 2, 3, and 5). These tests were conducted for Mach numbers M between 0.30 and 0.90, angles of attack α from -2.0° to 16.0°, and angles of side-slip β to 5.0°. The results of these tests helped to validate the SEADS algorithms at subsonic speeds and indicated that the performance of a FADS for the conditions tested was comparable to that of a conventional pitot-static probe system. This is an important result because flush-orifice installations have structural, cost, and weight advantages over pitot-static probe installations. Since these tests were performed, several aircraft were instrumented with all-flush-orifice air data systems by other flight test organizations to obtain air data (refs. 8 and 9).

The F-14 flight tests discussed in this report extended the data base to transonic and supersonic speeds and moderately high angles of attack and sideslip. The tests were conducted for Mach from M = 0.60 to 1.60, for angles of attack to α = 26.0°, and for angles of sideslip to β = 11.0°. The test results reported here provided flight verification data for the SEADS program and also provided a qualitative evaluation of the FADS concept, with emphasis at transonic speeds and high angles of attack.

For the F-14 tests, flush orifices were installed on a spherical nose cap surface in a cruciform pattern. The nose cap blended with the nose of the aircraft. Additional flush-mounted orifices were installed on the nose section aft of the nose cap. These orifices were installed to furnish a suitable static-pressure source to be used in conjunction with the orifices on the nose cap. They were also used to evaluate a FADS that cannot utilize orifices on the nose cap because of restrictions such as possible interference with radar units.

NOMENCLATURE

a_n normal acceleration at center of gravity, g

a_x longitudinal acceleration at center of gravity, g

a_y lateral acceleration at center of gravity, g

EKF   extended Kalman filter (nonlinear)

FADS   flush air data system

G.m.t.   Greenwich mean time

g   acceleration due to gravity

h_p pressure altitude, m and km

IR   infrared

LKF   linearized Kalman filter

M   free-stream Mach number

M_i indicated Mach number

PCM   pulse-code modulation

p   static pressure, N/cm^2; roll rate, deg/sec

p_i pressure measured at ith orifice, N/cm^2

p_t stagnation pressure, N/cm^2

p_3 to p_7 pressures measured at orifices 3 to 7 on nose cap, N/cm^2

p_{12} to $_{27}$ pressures measured at nose section orifices 12 to 27, N/cm^2

q   pitch rate, deg/sec

$\bar{q}$	dynamic pressure, N/cm^2
R	gas constant for air
r	yaw rate, deg/sec
SEADS	shuttle entry air data system
T	ambient temperature, °C
t	time, sec
V	true velocity, knots
WD	wind direction (direction from which wind is blowing), deg
WS	windspeed, knots
WS_z	vertical windspeed, knots
z	geometric altitude, m
α	angle of attack, deg
β	angle of sideslip, deg
ΔAP	differential pressure parameter used for angle-of-attack determination, N/cm^2
ΔBP	differential pressure parameter used for angle-of-sideslip determination, N/cm^2
Δh_p	change in computed pressure altitude due to change in ambient pressure, m
ΔM	$M - M_i$, Mach number correction for static-pressure position error; change in computed Mach number caused by change in ambient pressure
ΔV	change in computed true velocity due to change in ambient pressure, knots
θ	flow angle with respect to orifice, deg
ϕ	roll angle, deg
ζ	latitude angle of nose cap orifice, $\zeta = \alpha - \theta$, deg
ρ	density of air, gm/cm^3

FADS Pressure Parameters:

AP_{11}	angle-of-attack parameter, nose cap, $(p_7 - p_3)/\bar{q}$

3

AP_{12} angle-of-attack parameter, nose cap, $(p_6 - p_3)/\bar{q}$

AP_{21} angle-of-attack parameter, station 61, $(p_{14} - p_{12})/\bar{q}$

AP_{31} angle-of-attack parameter, station 127, $(p_{20} - p_{16})/\bar{q}$

BP_{11} angle-of-sideslip parameter, nose cap, $(p_8 - p_{11})/\bar{q}$

BP_{12} angle-of-sideslip parameter, nose cap, $(p_9 - p_{10})/\bar{q}$

BP_{21} angle-of-sideslip parameter, station 61, $(p_{15} - p_{13})/\bar{q}$

BP_{31} angle-of-sideslip parameter, station 127, $(p_{22} - p_{18})/\bar{q}$

BP_{32} angle-of-sideslip parameter, station 127, $[(p_{21} + p_{23}) - (p_{17} + p_{19})]/2\bar{q}$

PP_{22} static-pressure performance parameter, station 61, $(p_{12} + p_{14})/2p$

PP_{32} static-pressure performance parameter, station 127, $(p_{16} + p_{20})/2p$

PP_{3ALL} static-pressure performance parameter, station 127, $(p_{16} + \ldots + p_{27})/12p$

PTP_{14} stagnation pressure performance parameter, nose cap, p_4/p_t

PTP_{15} stagnation pressure performance parameter, nose cap, p_5/p_t

PTP_{16} stagnation pressure performance parameter, nose cap, p_6/p_t

Subscripts:

i   indicated

IR   measurement from probe on infrared scanner pod

m   measured

DESCRIPTION OF TEST AIRPLANE

The F-14 is a variable-geometry fighter-type aircraft (fig. 1). The particular airplane flown for the FADS tests was specially equipped to aid in a joint NASA and

U.S. Navy flight test demonstration of new flight control techniques (ref. 10). The special equipment included a pair of deployable, canard-like surfaces on the fuselage forebody for spin recovery (fig. 2). Although the canards were closed for the subject tests, they may have some effect on the upstream flow field because they are not flush with the airframe. In addition, the left side of the fuselage forebody has a gun fairing (fig. 2) that significantly disrupts the normal fuselage contour, whereas the right side has none. This geometric asymmetry may influence some of the pressure measurements.

A modified hemispherical pneumatic probe (fig. 3) for determining angles of attack and sideslip is usually installed on production aircraft (ref. 11). The flight test airplane was originally provided with a nose boom (fig. 1) for recording pitot-static pressure and flow-angle measurements. This nose boom was removed for the installation of the FADS sensor nose cap that was blended smoothly to the nose contours (fig. 4). In this way, in contrast to a probe installation, the FADS sensor was an integral part of the aerodynamic body of the airplane.

FLUSH AIR DATA SYSTEMS

The longitudinal axis of the nose cap (fig. 5) was aligned with the nose cone that was canted down 5.0° with respect to the longitudinal fuselage axis of the aircraft. Wing incidence was 0° relative to the fuselage centerline. The cap was polished to a surface roughness within 0.81 µm. Eleven orifices, 0.079 cm in diameter, were installed on the spherical surface of the nose cap. The orifices were drilled normal to the surface and were arranged in a cruciform pattern along the vertical and longitudinal body axes. Orifices along the vertical axis were placed at angular increments of 20°; those along the horizontal axis were placed at increments of 30°. Because of the necessarily small size of the spherical portion of the nose cap (8.38-cm diameter), the number of the orifices and the size of the connecting pneumatic lines (0.079-cm diameter) were restricted. The cruciform arrangement of the orifices was similar to those of the 14 SEADS nose cap orifices (ref. 4) and the 18 orifices mounted on the nose section of the KC-135 airplane (ref. 5).

The FADS pressure orifices on the nose section are shown in figure 6. These 0.318-cm-diameter orifices are located in two rows around the fuselage — a row of 4 orifices evenly spaced 61.0 cm aft of the nose apex and another row of 12 orifices 127.0 cm aft of the nose apex. (These distances are referred to as the station values, that is, stations 61 and 127.) The slope of the nose section relative to the nose cap apex changed from a nominal 60° at the base of the nose cap to 71° at station 61 and 77° at station 127. Nominal diameters of the nose section are 52 cm at station 61 for orifices 12 and 14 and 90 cm at station 127 for orifices 16 and 20. Because of the slightly noncircular cross-sectional shape of the nose section, the diameters applicable to individual orifices may differ by 2 or 3 percent from the nominal values.

These nose section orifices were included in the FADS test for two purposes: (1) to find one orifice or a combination of orifices that could provide a static-pressure source for accurate calibration and (2) to determine whether the use of other nose section orifices would be possible for accurate flow-angle measurements if orifice locations on the nose cap were not available. Such a FADS might be used

either as an independent system or in conjunction with a total-pressure probe. Figure 7 shows an internal view of the pressure lines, which varied in length from 1 to 3 m. They were made as short as practical and hence were not sized to equalize pneumatic lag.

REFERENCE MEASUREMENTS

Reference measurements for the FADS tests were supplied by a pitot-static probe equipped with flow-angle vanes (fig. 2). The probe, which was a standard NASA configuration (fig. 8 and ref. 12), was mounted on the infrared (IR) scanner pod and is referred to as the IR reference probe.

Position error corrections were obtained for the IR reference probe with the F-14 test nose boom in place (fig. 1) before installation of the FADS. The nose boom probe also had a standard NASA static-pressure orifice configuration. Measurements from the IR reference probe for angles of attack and sideslip were calibrated using the corrected vane measurements from the nose boom. The pitot-static-pressure measurements from the IR reference probe and the nose boom probe were calibrated by procedures outlined in appendix A. These procedures used pacer aircraft and radar measurements. Calibration curves are also presented in appendix A.

The position error corrections of the IR reference probe were checked for the effects of the nose boom removal during the two FADS test flights, using the techniques outlined in appendix A. The corrected static-pressure measurements from the reference system, as well as the other reference measurements, were verified by a trajectory reconstruction technique using a linearized Kalman filter (LKF). The technique combines data from several sources to achieve an enhanced result (ref. 13). These sources were onboard measurements, radar measurements, and upper air meteorological analyses. The onboard measurements included linear accelerations; pitch, roll, and yaw rates; roll angles; and air data. The radar measurements provided inertial velocity, altitude, and heading. The upper air meteorological quantities from rawinsonde measurements provided values of ambient pressure and temperature, as well as wind information. Required attitude (Euler) angles, which were not reliably measured on the aircraft, were estimated (app. B). Application of this trajectory reconstruction technique also provided independent reference values for free-stream static pressure and angles of attack and sideslip. Appendix C describes the upper air analysis.

INSTRUMENTATION

Absolute force-balance pressure transducers were used for the pitot-static-pressure measurements for the nose boom probe and the IR reference probe, as well as for sensing pressures from orifices 4 and 22. Most of the other FADS pressures were determined with the aid of differential pressure transducers that measured the difference between the pressure sensed at the particular orifice and that at either orifice 4 or 22. (Orifice 4 was used as the reference orifice for the FADS nose cap orifices 1 to 11; orifice 22 was used as the reference for the nose section orifices 12 to 27.) A differential pressure for these particular orifices was then added to the absolute pressure measured for the appropriate orifice (4 or 22). Only

6

differential pressure measurements were obtained for orifices 8 and 11 and for orifices 9 and 10; these were $p_8 - p_{11}$ and $p_9 - p_{10}$, respectively. Instrumentation problems precluded obtaining meaningful pressure measurements from orifices 1 and 2 (the two uppermost orifices on the nose cap).

A three-axis accelerometer mounted near the aircraft center of gravity measured the linear accelerations. Rate gyros measured pitch, roll, and yaw rates.

The instrument measurement uncertainties and the resolutions of the pertinent onboard recorded measurements are listed in table 1. The FADS pressure uncertainties for orifices using a reference transducer were obtained by adding the uncertainties of that transducer and those of the differential transducer. Uncertainties are based on the largest deviations in instrument calibration data of particular types of transducers used in the tests.

Data were recorded using a 10-bit pulse-code modulation (PCM) data recording system. The data were telemetered to the ground station and were also recorded on magnetic tape on board the airplane.

FLIGHT TESTS

Table 2 presents the test points obtained from the two flights used for FADS testing. Maneuvers flown for the FADS evaluation were (1) acceleration-decelerations at nearly constant altitudes for investigation of Mach number effects, (2) split-S and descending turns for investigation of angle-of-attack effects, and (3) rudder-induced sideslips. In addition, constant altitude and Mach number runs were made for checking the static-pressure calibrations of the reference air data system. Pacer calibration and "survey" data were obtained during these runs, as explained in appendix A.

The following ranges in the test variables were obtained: $M = 0.60$ to 1.60, $\alpha = -2.0°$ to $26.0°$, $\beta = -9.0°$ to $11.0°$, and Reynolds number/m = 3.3×10^6 to 1.8×10^7. High flow angles at high transonic speeds were limited. The data base provided by these maneuvers, although inadequate for complete calibrations, allowed a comprehensive evaluation of FADS suitability over much of the flight envelope of the airplane.

DATA ANALYSIS CRITERIA

The FADS pressure measurements were investigated to find a minimum or almost minimum set of pressure orifices that provided measurements from which all conventional air data quantities could be accurately derived for the F-14 configuration. This approach was similar to conventional air data measurement systems but was in contrast to the more elaborate procedure used to derive air data quantities using the SEADS algorithms. (In the latter case, instead of using the minimum or almost minimum set of orifices, all available orifices were used to obtain statistical derivations of the state variables.)

The SEADS approach is accomplished with the aid of a mathematical model based on modified Newtonian flow and empirical constants established from wind-tunnel

tests (ref. 6). Such a method is advantageous because it significantly reduces the risk of decreased accuracy, or even the loss of the associated parameter, in the event of the loss of any of the minimum set of pressure orifices. The SEADS pressure model can tolerate the loss of several measurements before the accuracy of any parameter is substantially degraded. For the shuttle case, this was particularly important because of the potential for damage in a severe operating environment. The SEADS testing routine rejects pressure measurements that are obviously contaminated.

The pressure measurements reported in this document were first examined for appropriateness in determining static pressure p, stagnation pressure p_t, angle of attack, and angle of sideslip to assess the general applicability of the FADS. (These are the quantities usually determined from a conventional pitot-static air data system.) Additionally, the determination of Mach number by nose cap pressure parameters was also investigated. The particular air data parameters investigated were consistent with those studied in the FADS program for the KC-135 airplane (ref. 5).

To select optimum orifices for determining the various air data quantities, time histories of the FADS pressure parameters were first investigated to study their behavior relative to Mach number and flow angles. Combinations of orifices were selected from both the nose cap and nose section arrays. The particular orifices selected for direct determination of stagnation pressure and static pressure were those that provided measurements least sensitive to Mach number and flow angle. The criteria used for the selection of particular FADS parameters were as follows: (1) parameter sensitivity to the air data quantity to be derived and parameter insensitivity to other quantities, (2) repeatability and accuracy, and (3) simplicity of functional relationships.

Data plots presented in this report are for measurements from selected orifices. The quantities plotted for evaluation of stagnation pressure and static pressure are simply the ratios of the measured FADS pressure (or average FADS pressure) to reference stagnation pressure and static pressure, respectively. Angle-of-attack and angle-of-sideslip parameters are simply the ratios of the difference of two FADS pressures (or the difference between averaged pressures) and dynamic pressure. These parameters were also used for the FADS program for the KC-135 airplane (ref. 5). The Mach number parameters investigated are the ratios of pairs of FADS pressure measurements from the nose cap.

The FADS data curves are only for evaluation of the appropriateness of FADS parameters at transonic speeds and at moderately high flow angles. They are not intended to be applicable as calibration curves. After calibration curves are established for such a system, various data reduction schemes are available (refs. 14 to 17).

RESULTS AND DISCUSSION

Confirmation of Reference Conditions

The primary calibration data for the position error of the IR reference probe were obtained with the test nose boom installed during flights prior to the FADS

flights. To define any significant changes in the position error with the removal of the nose boom, additional calibration data were obtained during the FADS testing.

Representative static-pressure position error data for the IR reference probe with the nose boom removed are shown in figure 9. The quantity ΔM in figure 9 was the Mach number correction for static-pressure position error. The calibration curve (solid line) was generated from data obtained with the nose boom installed. Data obtained with the nose boom removed are shown for three methods of analysis: the radar method, the pacer method, and the LKF reconstruction method. The LKF measurements were taken at the same time as the pacer measurements. The data from the three methods, although showing some consistent differences, agree within ±0.01 of the calibration curve. Some differences between the measured data and the calibration curve can be attributed to differences in the angles of attack for which the data were taken. For the purposes of this report, the data substantially confirmed the calibration curve.

Further confirmation of the static-pressure calibration curve, as well as the other reference calibration data, was obtained from the comparison plots shown in figure 10. These plots provide typical time histories of quantities obtained from the LKF reconstruction, the fully corrected IR reference probe data, and the upper air wind values obtained by analysis of rawinsonde data. The time histories included a split-S maneuver and a maneuver that resulted in elevated angles of attack and sideslip. A pullup maneuver began at 135 sec, the split-S maneuver began at 165 sec, and the manuever for combined angles of attack and sideslip began at 310 sec.

The difference in sideslip angle indicated in figure 10(d) changed sign during execution of the split-S maneuver. This change occurred when the airplane heading changed by 180° and hence was primarily due to a discrepancy between the LKF-derived lateral components of the wind and the actual values. The LKF sideslip values were sensitive to the lateral velocity and the heading angle. Some bias error existed in the reconstructed heading angle. Figures 10(g) and 10(h) show that the windspeed WS difference was as large as 9 knots and the wind direction WD difference was on the order of 10°. As noted in appendix C, a significant part of the differences in windspeed and wind direction may result from uncertainties due to measurement error and atmospheric variability.

Evidence of LKF errors during the highly dynamic maneuvers was demonstrated by the large LKF vertical windspeed values during these maneuvers, as plotted in figure 10(f); lower values resulted at other times. Of course, vertical windspeed measurements were not determined from rawinsonde measurements and were normally, as for this flight, assumed to be close to zero. In general, however, the differences between the LKF and the IR reference probe curves were relatively small.

The mean differences between the LKF and the IR reference probe values were as follows: Mach, ±0.01; pressure altitude h_p, ±6 m; dynamic pressure $\bar{q}$, ±0.048 N/cm^2; α, $\pm0.5°$; and β, $\pm1.0°$. These differences were considered to represent the uncertainty in the original air data calibration curve for application to the FADS study.

9

Characteristics and variations of the FADS pressures and derived quantities, especially those associated with the nose cap measurements, are discussed here. First, several test maneuver time histories of FADS pressures are given a cursory examination for applicability to air data determination. Second, the nose cap pressures from a transonic acceleration are presented to show that they did not display a Mach discontinuity, as would be the case for a nose-mounted pitot-static probe. Finally, the nose cap pressure distributions measured from orifices in the vertical plane are compared with theoretical values for various Mach numbers and angles of attack. A similar comparison is not presented for the orifices downstream of the nose cap, because the more complex flow field was not modeled.

Typical time history. — Figure 11 shows a 280-sec time history of FADS pressures and reference air data values during which an acceleration, a sideslip maneuver, and a split-S maneuver were performed. As shown in figure 11(a), M = 0.67 to 1.32; as shown in figure 11(b), h_p = 11.7 to 12.9 km. As shown in figures 11(c) and 11(d), respectively, maximums of β = 5.0° and α = 10.0° were reached at supersonic speeds.

Time histories such as those provided in figure 11 quickly indicated which pressures were most useful for determination of some air data quantities. For example, p_6 showed the most sensitivity to angle of attack; see figure 11(j) for values near 240 sec. Hence, p_6 could be a useful measurement for angle-of-attack determination. Both differential pressures $p_8 - p_{11}$ and $p_9 - p_{10}$ in figures 11(l) and 11(m), respectively, appear suitable for determining angle of sideslip because of their large variations during the sideslip maneuver between 214 and 230 sec. The determination of Mach number, stagnation pressure, and static pressure requires more detailed studies for selection of appropriate orifices and is discussed in the Evaluation of FADS Sources section of this report.

Nose cap pressures at transonic speeds. — Figure 12 shows time histories of the FADS pressures measured from the orifices on the vertical centerline of the nose cap for an acceleration from M = 0.98 to 1.04. In this transonic range, static-pressure measurements from nose-mounted probes are subject to pressure or Mach discontinuities. This is true even for probes that are "compensated" to minimize errors at these Mach numbers (ref. 18). However, such discontinuities were not evident from the FADS pressures, which indicated that the bow wave was detached from the nose. Calibrations of similar flush-orifice nose installations do not have to account for such discontinuities and consequently offer improved accuracy.

Nose cap pressure distribution. — Several theoretical and empirical approaches reported in the literature were found to define the pressure distribution on a sphere. However, to provide an accurate air data system, hemispherical sensors must always be calibrated (ref. 16). For example, the algorithms for SEADS were based on wind-tunnel data empirically adapted to a mathematical model based on modified Newtonian flow theory, which is most accurate at hypersonic speeds.

Figure 13(a) shows the ratio of the pressure measured at the ith orifice to the stagnation pressure (p_i/p_t) as a function of latitude angle ζ of the nose cap, as predicted by modified Newtonian flow for a spherical body. Curves are shown for

M = 0.619, 0.908, and 1.250 for comparison with flight data obtained at $\alpha = 5.0°$. All predicted curves had a maximum pressure ratio of 1.0 at $\zeta = 5.0°$, to account for the nose cap being canted down 5.0° from the mean aerodynamic chord of the airplane. Flight-determined pressure ratio values were obtained for a range of Mach numbers including those referenced. The data agreed fairly well with the curves for Newtonian flow for $\zeta < 45.0°$. Above $\zeta = 45.0°$, the theory underpredicted the level of the measured pressures. The discrepancies increased with Mach number; however, good correlation was not expected for the higher angles because orifice 7 was close to the point at which the sensor surface was not spherical (fig. 5).

Figure 13(b) shows flight data values of p_i/p_t plotted with latitude angle. These data are for five angles of attack in approximately 5° increments. The ratio of p_i/p_t was expected to be 1.0 when $\zeta = \alpha$ (that is, flow angle $\theta = 0°$).

This appeared to be true for the curves for the two lower angles of attack. However, the maximum shifted to higher latitude angles for $\alpha = 15.0°$ or more. The shift, which became more pronounced as latitude angle increased, may be attributable to upwash and possible viscous effects.

Evaluation of FADS Sources

Stagnation pressure. — Only orifices on the vertical centerline of the nose cap were considered (specifically, orifices 4 to 6) for the determination of stagnation pressure. The measurements from these orifices were not significantly affected by sideslip during nonmaneuvering flight and were expected to provide pressures near values of stagnation pressure for limited ranges of angle of attack. Figure 14 shows the stagnation pressure parameter PTP as a function of Mach for one acceleration-deceleration test flight from $\alpha = 0°$ to 5.9°. For orifice 4, PTP_{14} was very insensitive to Mach for this angle-of-attack range, especially in comparison to the other two parameters. This was to be expected because for orifice 4 throughout this test, $\theta < 6°$.

Variations of these pressure ratios with angle of attack are shown in figure 15 for three different Mach ranges. Figure 15(a) shows data for two test flights from M = 0.57 to 0.68. Parameter PTP_{14} indicated little sensitivity up to $\alpha = 10.0°$, again because of the relatively small flow angle for orifice 4. Parameter PTP_{15} had a maximum value and less sensitivity near $\alpha = 15.0°$. The quantity associated with the orifice that had the largest latitude angle, PTP_{16}, exhibited less sensitivity near $\alpha = 26.0°$. These results illustrated that for cases in which angle-of-attack corrections are not practical, orifices could be selected for the direct measurement of stagnation pressure with angle-of-attack variations producing only small errors.

Large scatter in the figure 15(b) data from M = 0.87 to 0.92 was attributed to two sources: (1) as noted in figure 14, when flow angle was large, the pressure ratios were significantly affected by Mach; and (2) the data were affected by pneumatic lag that resulted from small orifices, relatively small diameter pressure lines, and high angle-of-attack rates. Significant lag was also reported for a hemispherical probe system in reference 19. Some data in figures 15(b) and (c) were obtained at decreasing angle-of-attack rates as high as 18 deg/sec. Rates for

increasing angle of attack, at relatively constant Mach, were considerably less. Hence, only these data were representative for indicating variations of stagnation pressures with angle of attack.

Variations in PTP with sideslip are shown in figure 16(a) for M = 0.75 to 0.80 and in figure 16(b) for M = 0.87 to 0.92. Each of the three PTP ratios resulted in about a 3-percent variation over the sideslip range shown. Variations in PTP with angle of sideslip were expected to be small for orifices 4 to 6.

A well-designed pitot probe has an advantage over flush-orifice systems in that it can be rather insensitive to quite large flow angles (ref. 20). However, if flow angles are not too large, the corrections needed for a flush-orifice system may be small, well defined, and correctable, as shown.

Static pressure. — Unlike the determination of stagnation pressure, direct static-pressure measurement was not practical from any of the nose cap orifices, because they were not perpendicular to the flow direction for most flight conditions. Therefore, only orifices downstream of the nose cap were considered for sensing static pressure. Use of flush static orifices is quite common, especially on large aircraft. However, their use on aircraft at transonic speeds and at high flow angles has been limited.

The three most promising ratios for static-pressure performance parameters PP were PP_{22}, PP_{32}, and PP_{3ALL}. The pressures used in determining these parameters were measured individually. For example, the value of PP_{22} was obtained by averaging the static pressures from orifices 12 and 14 and dividing by the free-stream static pressure; that is, $(p_{12} + p_{14})/2p$. On an operational system, the two orifices could be manifolded to obtain a pneumatic average.

Figure 17 presents the variations in the three selected ratios with respect to Mach. The ratio for parameter PP_{22} had the largest sensitivity to Mach but had a smooth, well-defined variation. The other ratios had smaller variations with Mach but showed effects of more complex, and possibly shock-induced, flow fields.

Variations of the pressure ratios with angle of attack for M = 0.60, 0.90, and 1.23 are shown in figures 18(a) to 18(c). Scatter in the data was primarily due to Mach variations. An attempt to correct the pressure ratios to constant Mach by fairing the data from figure 17 was not very successful, probably because the dependency of the ratio on Mach varied substantially with angle of attack.

Figures 18(a) and 18(b) for the two lower Mach values show that PP_{22} had the smallest variation with angle of attack — less than 3 percent from $\alpha = 2.0°$ to 26.0°. Performance parameter PP_{32} showed a much larger variation than PP_{22} but appeared to be better than PP_{3ALL}. As indicated in figure 18(c), at supersonic speeds, all three pressure ratios were sensitive to angle of attack.

Variations of the static-pressure ratios with angle of sideslip for two limited Mach ranges are shown in figure 19. All these variations were small, had little data scatter, and resembled variations with sideslip experienced in the stagnation pressure ratios.

12

The qualitative evaluation for the flow angles and Mach ranges considered in this study indicates that the PP_{22} ratio was most suitable for determining static pressure. However, more intensive effort is required for accurate calibration of the static source associated with this parameter. Such an effort should include wind-tunnel testing.

Angle of attack. — In figure 20, four pressure parameters AP for determination of angle of attack are plotted with attack angle for M = 0.60, 0.90, and 1.23. Parameters AP_{11} and AP_{12} corresponded to pairs of nose cap orifices in the vertical plane. Parameter AP_{21} used the top and bottom nose section orifices at station 61; parameter AP_{31} used similarly located orifices at station 127. To avoid the pneumatic lag effects previously mentioned, data associated with large angle-of-attack rates were not plotted in figure 20.

Past studies (ref. 14) show that the relationship of these parameters to angle of attack is fairly linear to relatively large angles. Most plots in figure 20 showed good linearity; exceptions were those for AP_{11} at low angles and all parameters at supersonic speeds. A more important consideration for determining angle of attack, of course, was parameter sensitivity to angle of attack. As expected, the largest sensitivities (largest slopes) were for the nose cap parameters. Sensitivity decreased for parameters measured at orifices located at greater distances from the nose cap. In general, data scatter was relatively small. When the angle-of-attack parameters were plotted as a function of sideslip angle (fig. 21), a slight dependency on sideslip resulted for all the parameters.

Figure 22 shows the variation of angle-of-attack parameters with Mach for α = 0°, 4.0°, and 8.0°. The parameters that had the largest angle-of-attack sensitivities were those associated with the nose cap. Sensitivity to Mach number depended on angle of attack and changed substantially as Mach increased from approximately M = 1.10 to 1.30.

Figure 23 shows angle-of-attack sensitivity of the four parameters as a function of Mach. Sensitivity values were obtained by taking the differences of the values of the parameters at the extreme angle-of-attack values of figure 20 and dividing them by the angle-of-attack change. Although the nose cap parameters demonstrated the highest sensitivity to angle of attack, they also had the largest sensitivity to Mach; AP_{12} had the largest variation. From this investigation, it appeared that tradeoffs must be made between parameter sensitivity to angle of attack and unwanted sensitivity to Mach.

As shown in figure 23, the sensitivities for a small hemispherical probe with orifices spaced 90° apart (ref. 21) agreed reasonably well with those for AP_{11}, for which the associated orifices were spaced 80° apart. Considerable care must be taken in the transonic region for adequate calibration of an angle-of-attack sensor utilizing pressure orifices on a spherical surface. Of course, such care is necessary for any air data sensor. Sensitivities associated with the other orifices aft of the nose cap were considerably less and were less than typical sensitivities for various flow-angle sensors used for measurements in incompressible flow (ref. 16).

From this study, it was concluded that angle of attack could be determined from pairs of orifices located on the nose cap or at either of the two nose section stations.

Angle of sideslip. — Figure 24 shows the variations of five pressure parameters BP with angle of sideslip for determination of sideslip at two Mach values. Supersonic data were not included because significant changes in sideslip were not achieved during the supersonic testing. Very linear relationships were achieved for all parameters.

Figure 25 shows the parameter sensitivities to sideslip plotted with Mach. It also shows AP sensitivities determined in this study. Parameters AP_{21} and AP_{31} were expected to be comparable to parameters BP_{21} and BP_{31} because of similar orifice spacing. Indeed, as shown in figure 25, good agreement was generally achieved for the analogous sensitivities. Parameters for the nose section orifices were in closest agreement.

Mach number. — If pressure measurements were restricted to the nose cap, a static-pressure measurement would not be available for Mach number determination. Simple pressure ratios from measurements on the nose cap were investigated to determine Mach (refs. 3 and 5). The two most promising ratios for this study, P_3/P_6 and P_3/P_7, were plotted with Mach at low angles of attack (fig. 26). The pressure ratio P_3/P_6 was not very sensitive to Mach between M = 0.70 and 1.10 and above M = 1.35. Hence, this pressure ratio could not provide an accurate determination of Mach. The ratio P_3/P_7 had adequate sensitivities for the entire Mach number range shown in figure 26. In fact, excellent sensitivity occurred above Mach 1.10. (Above Mach 1.37, data were not available because of transducer saturation for the P_7 pressure measurement.) From the angle-of-attack evaluation, both ratios were also found to be sensitive to angle of attack. Hence, angle of attack had to be accurately determined before Mach could be ascertained.

Unfortunately, instrumentation problems precluded obtaining pressure measurements from orifices 1 and 2. Data in reference 3 indicated that these pressure measurements would provide Mach parameters that were less sensitive to angle of attack at the higher attack angles. Ratios such as P_1/P_6 and P_2/P_7 should therefore be more accurate than either ratio P_3/P_6 or P_3/P_7 for Mach determination. Nevertheless, Mach determination was attainable with FADS even when good static-pressure sources were not available.

Selection of FADS Orifices

Several combinations of orifices were available for providing means of air data determination. Table 3 lists the best combinations of orifices, according to location, for the determination of the air data quantities. Table 3 (last row of table) also includes the best orifice or combination of orifices, regardless of location, for all the air data measurements. Selection of the orifices was based on the criteria stated in the DATA ANALYSIS CRITERIA section of this report.

For the measurement of stagnation pressure (at least in the conventional sense) at moderate angles of attack, only orifice 4 is recommended. However, for $\alpha > 25.0°$, orifices 5 and 6 would be better sources. Orifice 5 should be used for intermediate angles, and orifice 6 for higher angles. A direct static-pressure measurement was not available on the nose cap; the best source for this

14

measurement was provided by the arithmetically averaged pressures from the top and bottom of the nose section at station 61. Pneumatic manifolding of the two orifices should also achieve the same result.

Determination of angle of attack was provided by pairs of orifices located on the nose cap and at both stations on the nose section. The nose cap provided angle-of-attack parameters with the largest sensitivities. Orifice pair 3 and 7 was judged the best for angle-of-attack determination on the nose cap, although orifice pair 3 and 6 was also acceptable. Orifice pairs for the downstream locations provided parameters with considerably lower sensitivities, but with suitable accuracy if proper resolution was provided in sensing the pressures. For example, if a 10-bit PCM instrumentation system was required to provide adequate resolution for angle-of-attack determination from orifices on the nose cap, a 12-bit PCM system was similarly required for orifices at station 127. This is because the differential pressure measured between a pair of orifices is directly proportional to the sensitivity factor.

All locations had pairs of orifices that adequately provided the means for determining angle of sideslip with proper instrumentation; the nose cap provided the optimum pressure sensitivity.

The only pressure parameter found for Mach determination was the ratio of pressures measured from orifice pair 3 and 7 on the nose cap; first, however, angle of attack had to be accurately determined. Use of such a parameter resulted in reduced accuracy at transonic speeds (ref. 4). Better accuracy was achieved if static pressure was measured on the nose section and combined with stagnation pressure measured on the nose cap. If pressure measurements were confined to the nose cap, additional pressure ratios determined from orifice pair measurements could be made to take advantage of statistical means for obtaining an enhanced result.

CONCLUDING REMARKS

A flight test investigation was made to evaluate a flush air data system (FADS) with all flush orifices for use at transonic speeds and at moderately high flow angles. Orifices were located in three areas on an F-14 airplane. One group of orifices was installed on the spherical surface of a specially constructed nose cap that was blended smoothly to the contours of the airplane nose section. Orifices were also installed at two different locations (stations 61 and 127) on the nose section. Measurements were obtained between Mach 0.60 and 1.60, between -9.0° and 11.0° angle of sideslip, and to a maximum 26.0° angle of attack.

With careful calibration, a FADS can provide accurate air data information at transonic speeds and over a large range of flow angles. In general, the pressure field of the nose cap was less complex than the pressure field at the other orifice locations on the nose section. For example, no Mach discontinuity was found on the nose cap, indicating that the bow wave of the aircraft was detached. Hence, at Mach numbers for which discontinuities occur on a pitot-static probe on the nose boom, a more accurate air data determination is possible with flush orifices on a nose cap than with the nose boom probe. The pressure distribution on the spherical portion of the nose cap compared favorably with that predicted by Newtonian flow for a spherical body.

Several orifices on the nose cap were suitable for accurate determination of stagnation pressure. The pressures from these orifices were moderately dependent on flow angle but, because of good repeatability, were correctable.

Orifices on the forward location (station 61) on the nose section were found to be more suitable for the determination of static pressure than the other orifice locations. However, more calibration effort would be required if these orifices are to provide accurate determination of static pressure.

Pairs of orifices on the nose cap provided the best means of determining angle of attack because they provided the largest pressure sensitivities with angle of attack. The sensitivities of the orifice combinations investigated downstream of the nose cap were typically less than conventional flow-angle sensors. However, they provided accurate flow angle information with suitably accurate instrumentation. The parameter sensitivities were found to vary considerably with Mach in the transonic range; the larger the general levels of sensitivity, the more the sensitivities varied with Mach. Because of the relatively large sensitivity variations with Mach, careful calibration of the pressure parameters is required at these speeds. The general findings that applied to angle-of-attack determination through pressure measurements are also applicable in principle for the determination of angle of sideslip.

APPENDIX A — POSITION ERROR CALIBRATIONS AND CORRECTIONS

The reference air data probe (IR probe) was calibrated using the pacer and acceleration-deceleration methods. The acceleration-deceleration method is described in reference 22; the analysis of upper air pressure heights required for this method is described in appendix C. To provide additional information on pressure heights and to check the radar altitude accuracy (ref. 23), constant Mach runs were made along the same ground track and at the same altitude as the acceleration-deceleration runs.

Figure 27 shows static-pressure position error data at low angles of attack. These data were obtained with the nose boom installed instead of with the FADS nose cap. Good agreement was achieved between the pacer and acceleration-deceleration techniques. The final curve for Mach number correction ΔM for static-pressure position error for low angles of attack, which was based on more data than that included in figure 27, is presented in figure 9. As indicated in figure 28, angle-of-attack effects on the static-pressure error were significant. The numbers at the data points in figure 28 are the corresponding values of indicated Mach number M_i. From such data, correction curves were generated (fig. 29). The curves for each indicated Mach were adjusted so that $\Delta M = 0$ at the average angle of attack flown for the position error calibration data at lower attack angles. This was done for the purpose of data reduction.

The IR reference probe static-pressure correction for position error also varied significantly with angle of sideslip, as indicated in figure 30. Here, a typical plot of ΔM variation in a sideslip maneuver is shown for $M = 0.60$ and $\alpha \approx 5.0°$.

A comparison of the stagnation pressures from the nose boom pitot-static probe and the IR reference probe indicated large differences above $M = 1.00$. Figure 31 shows the IR reference probe stagnation pressure plotted as a function of indicated Mach for three flights. The variation was found to be independent of angle of attack below $\alpha = 10.0°$. Lack of supersonic data above $\alpha = 10.0°$ prevented a similar stagnation pressure calibration for the higher flow angles.

Calibrations for angles of attack and sideslip were obtained by comparing nose boom vane and IR reference probe values. The indicated angle-of-attack values for the nose boom system were corrected for pitch velocity, upwash, boom and fuselage bending, and probe misalignment with the mean chord line of the wing. The IR reference probe indicated angular measurements were corrected only for aircraft angular velocities. Figure 32 shows typical comparisons of the angular measurements. From the IR reference probe calibration data, sidewash effects were probably a consequence of the gun fairing (fig. 2). From the calibration data, tabular listings of corrections were constructed and used in a computer program to obtain the free-stream air data quantities. Linear interpolation was used to obtain correction values between tabular entries.

APPENDIX B — RECONSTRUCTION OF AIRCRAFT ATTITUDE ANGLES

A malfunction in the gimbaled inertial platform necessitated the reconstruction of the aircraft pitch, roll, and yaw angles (Euler angles) from other data sources. These sources included body-axis linear accelerations and angular rates, wind-relative flow angles, meteorological data, and radar tracking data. The basic approach was to integrate attitude rate gyro data and to correct for bias-caused drift using meteorological data, wind-relative flow angle data, and tracking data. The integration was performed using an extended (nonlinear) Kalman filter (EKF). The reconstructed values for the attitude angles were believed to be of comparable quality to data obtained from the gimbaled platform. All computations were performed postflight.

The first step of the method was the calculation of rough estimates of the aircraft attitude angles using the wind-relative flow angle, meteorological, and tracking data. The wind-relative flow angle data were obtained from the IR reference probe. The meteorological data were obtained from atmospheric analyses of rawinsonde balloon data (app. C), and the tracking data were obtained from the NASA-Dryden AN/FPS-16 (C-band) high-range tracking system (ref. 23). Flightpath heading and flightpath angle were algebraically combined with angle of attack, sideslip, and wind heading to give the rough estimates. The geometry, although tedious, is straightforward (ref. 24). This calculation was performed at the rate of 0.5 sample/sec.

The second step of the method was to integrate the rate gyro data using an EKF (ref. 25). The integration was performed at the rate of 25 samples/sec; updates to correct for bias-caused drifts were performed at the rate of 0.5 sample/sec. The updates were performed using the rough estimates described in the previous paragraph. Essentially, the EKF was used to superimpose the high-frequency inertially derived information on the rough estimates of the attitude angles.

Because the updates were performed only once every 50 samples, the data tended to take on a sawtooth appearance when plotted, which is obviously artificial. This problem was alleviated by passing the filtered estimates back through a fixed-interval optimal smoother (ref. 25). This smoother eliminated the saw-toothed edges while preserving the frequency content of interest. The plots of the resulting final estimates took on a smooth appearance. Figure 33 presents an example of the rough, filtered, and smoothed estimates for roll attitude. All values had the same mean trend; however, the frequency content of each was clearly different.

18

APPENDIX C — METEOROLOGICAL UPPER AIR ANALYSIS

Background

The primary purpose of using upper air analysis for air data calibration was to establish a good estimate of ambient pressure as a function of geometric altitude. Synoptic upper air data obtained from several locations at given times (for 00:00 and 12:00 hr Greenwich mean time, G.m.t.) were charted with isolines and analyzed to depict the pattern of pressure altitude, temperature T, and wind fields. Changes in both value and pattern of the upper air pressure, temperature, and wind fields were conveniently observed from these charts. Principal attention was placed on the pressure field because the airplane static-pressure source error is the main cause of error for in-flight measurement of pressure altitude, Mach, and airspeed.

Examples of pressure altitude, Mach, and airspeed sensitivity to the accuracy of the ambient pressure are presented in table 4. For these examples, a pressure increment equal to 0.1 percent of the ambient pressure is shown. The sensitivity of Mach and airspeed to pressure or altitude accuracy decreases with Mach at subsonic speeds. It reaches a minimum transonically at $M = 1.14$ and then increases with Mach above this value. The sensitivity does not change with altitude between $h_p = 11.00$ and 20.00 km. Therefore, only a few flight conditions are needed to represent the sensitivities for a wide range of transport and fighter aircraft, as indicated in table 4.

Both onboard pressure sensors and ground-based tracking radar were available with accuracy and precision comparable to 0.1 percent of the pressure, or better. The typical accuracy of individual upper air measurements was more likely to be in the range of 0.5 to 1.0 percent of the ambient pressure. Therefore, meteorological analyses were performed to provide estimates that minimized the errors due to measurement accuracy as well as errors due to variability in time and space.

Upper Air Measurements

Upper air data were obtained by rawinsonde methods that combined wind determination by radar or radio direction-finder techniques (rawin) with temperature, humidity, and pressure determination using a balloon-borne sensor package (radiosonde). For a specific system used at a particular upper air station, the relation between pressure and geometric altitude z may be obtained by one of two methods. The most prevalent method has been to measure pressure, temperature, and humidity directly on the sonde instrument. Density ρ is derived from these measurements by the equation of state, and altitude is subsequently derived by integration of the hydrostatic equation,

$$\delta p = -\rho g \, \delta z$$

or, in terms of the measured independent variables,

$$\int_{z_o}^{z} \delta z = -\int_{p_o}^{p} \frac{RT}{g} \delta(\ln p)$$

where g and R represent the acceleration due to gravity and the gas constant for air, respectively. With this method, a radio direction-finder antenna is used for tracking. The elevation angle and derived altitude are coupled with the measured azimuth angle to determine the range, location, and winds.

In recent years, tracking systems that directly measure range (radar) and altitude have come into use. Sounding instruments that do not measure pressure directly may be employed with these systems. For such systems, the equations of state and hydrostatic balance are rearranged so that pressure becomes the dependent variable. Pressure is measured independently at the station location by a ground-based barometer and is used to initialize the integration,

$$\int_{p_0}^{p} \delta(\ln p) = -\int_{z_0}^{z} \frac{g}{RT} \delta z$$

Meteorological Analysis Procedure

Analyses of the upper air data are accomplished by interpolation of the data in (geographical) space for given pressure values (mandatory reporting levels). These data fields may include temperature, humidity, and winds, as well as the height of the pressure surface being analyzed. As shown in figure 34, the fields are usually depicted by isolines or height contours (solid lines) and by isotherms (broken lines). Whether the analyses are produced objectively with a machine or manually with subjective judgment, fitting the data to a consistent weather pattern reduces the effect of random measurement errors and can thereby help to eliminate the effects of data from excessively biased sensors. The data are interpolated to the test site location on the synoptic charts analyzed.

The next steps in the procedure are to examine the vertical consistency of the analyses and to interpolate the data to the test time for the individual mandatory pressure levels. The differences between geometric altitude and pressure altitude $(z - h_p)$ are therefore plotted as a function of altitude. These differences are used to depict the pressure field at the test site. The $z - h_p$ quantity identifies the differences in pressures between the test day and the standard day, as defined by reference 26, for position error calibration purposes. The quantity $z - h_p$ is a convenient value to convert geometric altitude measured by radar to pressure altitude, $h_p = z_m - (z - h_p)$, and subsequently to convert it to ambient pressure.

Figure 35 shows the $z - h_p$ profiles for the two FADS flights. The morning and afternoon synoptic analyses showed reasonably consistent trends with altitude. These profiles were then linearly interpolated to the flight test times for the two flights reported here. On the basis of surface pressure measurements, subjective adjustments of the atmospheric semidiurnal tide were also applied to the linear interpolated $z - h_p$ values. These adjustments were equivalent to 9 and 2 m, respectively, for the test times. (On days when the upper air fields contained small-scale features in the pattern or fronts advecting through the test area, additional adjustments to the linear interpolation were warranted. The semidiurnal adjustment was relatively subjective, given the lack of suitable observation and applied theory.)

20

Edwards AFB rawinsonde data observed between the test times agreed well with the interpolated $z - h_p$ profiles below $h_p = 9.10$ km. Temperatures measured on this rawinsonde between $h_p = 9.10$ and 12.20 km were anomalously cool. Above $h_p = 9.10$ km, these cooler temperatures produced lower $z - h_p$ values than did the synoptic analysis. Because these cooler temperatures were not confirmed by other available rawinsondes from Edwards AFB and nearby upper air stations, the interpolated $z - h_p$ values were left as analyzed and not adjusted on the basis of the local observation.

Accuracy expected for the $z - h_p$ profiles on the test day ranged from better than ± 9 m below $h_p = 9.10$ km to ± 23 m above $h_p = 12.20$ km. These $z - h_p$ profiles were used with radar altitude to provide an independent reference air data calibration.

To maintain the accuracy of the $z - h_p$ values used for flight data at nominal distances from Edwards AFB, corrections were applied for the horizontal gradient of $z - h_p$. Values for these corrections were estimated (ref. 22) on the basis of the gradients on the mandatory level analyses and by applying the geotrophic flow approximation to the windspeeds. For these FADS flight tests, the estimated gradients in $z - h_p$ ranged from less than 0.15 m/n. mi. below $h_p = 4.60$ km to more than 0.30 m/n. mi. between $h_p = 9.10$ and 12.20 km. The directions of $z - h_p$ decrease range from northerly at $h_p = 1.50$ km to east-northeasterly at $h_p = 12.20$ km.

Temperature and winds were also analyzed in a similar manner when radar velocities were used for air data calibration techniques using true airspeed or Mach, such as the LKF technique described in appendix B. When local rawinsonde observations were available, the estimated wind and temperature profiles were weighted less heavily on the synoptic chart analyses than was the case for the $z - h_p$ profiles. On the test day, the expected accuracy of the temperature estimates ranged from ± 1.0 to $\pm 3°C$. Errors in the estimated wind components were expected to be less than 3 m/sec. Mach number uncertainties due to these effects are on the order of ± 0.003 (0.001 to 0.005) Mach for temperature and ± 0.01 Mach due to wind error.

REFERENCES

1. Larson, Terry J.; and Schweikhard, William G.: Use of the Shuttle Entry Air
    Data Pressure System at Subsonic Speeds. Proc. Second Biennial Air Data
    Systems Conference, May 1978, pp. IV-8-1 to IV-8-7.

2. Larson, Terry J.; and Siemers, Paul M. III: Subsonic Investigation of an All
    Flush Orifice Air Data System. Proc. 1980 Air Data Systems Conference,
    U.S. Air Force Academy, Colorado Springs, CO, 1980.

3. Larson, Terry J.; Flechner, Stuart G.; and Siemers, Paul M. III: Wind Tunnel
    Investigation of an All-Flush-Orifice Air Data System for a Large Subsonic
    Aircraft. NASA TP-1642, 1980.

4. Larson, Terry J.; and Siemers, Paul M. III: Use of Nose Cap and Fuselage
    Pressure Orifices for Determination of Air Data for Space Shuttle Orbiter
    Below Supersonic Speeds. NASA TP-1643, 1980.

5. Larson, Terry J.; and Siemers, Paul M. III: Subsonic Tests of an All-Flush-
    Pressure-Orifice Air Data System. NASA TP-1871, 1981.

6. Pruett, C.D.; Wolf, H.; Heck, M.L.; and Siemers, Paul M. III: An Innovative
    Air Data System for the Space Shuttle Orbiter — Data Analysis Techniques.
    AIAA-81-2455, 1981.

7. Siemers, P.M. III; Wolf, H.; and Flanagan, P.F.: Shuttle Entry Air Data System
    Concepts Applied to Space Shuttle Orbiter Flight Pressure Data To Determine
    Air Data — STS 1-4. AIAA-83-0118, 1983.

8. Brown, E.N.; Friehe, C.A.; and Lenschow, D.H.: The Use of Pressure Fluctu-
    ations on the Nose of an Aircraft for Measuring Air Motion. J. Climate and
    Applied Meteorology, vol. 22, no. 1, Jan. 1983, pp. 171-180.

9. Bowen, S.W.; Scott, S.G.; Chan, K.R.; and Borucki, J.G.: Yaw and Angle of
    Attack Measurements on the NASA CV-990 Aircraft. AIAA-85-0341, 1985.

10. Gera, J.; Wilson R.J.; Enevoldson, E.K.; and Nguyen, L.T.: Flight Test
    Experience With High-α Control System Techniques on the F-14 Airplane.
    AIAA-81-2505, 1981.

11. Larson, Terry J.: Evaluation of a Flow Direction Probe and a Pitot-Static
    Probe on the F-14 Airplane at High Angles of Attack and Sideslip. NASA
    TM-84911, 1984.

12. Richardson, Norman R; and Pearson, Albin O.: Wind-Tunnel Calibration of
    a Combined Pitot-Static Tube, Vane-Type Flow-Direction Transmitter, and
    Stagnation-Temperature Element at Mach Numbers From 0.60 to 2.87. NASA
    TN D-122, 1959.

13. Whitmore, Stephen A.: Reconstruction of the Shuttle Reentry Air Data
    Parameters Using a Linearized Kalman Filter. AIAA-83-2097, 1983.

14. Beecham, L.J.: The Hemispherical, Differential Pressure Yawmeter at Super-
    sonic Speed. R.&M. No. 3237, Deputy Controller Aircraft (Research and
    Development), Ministry of Aviation, Her Majesty's Stationary Office
    (London), 1960.

15. Bryer, D.W.; and Pankhurst, R.C.: Pressure-Probe Methods for Determining
    Windspeed and Flow Direction. National Physical Laboratory, Dept. of
    Trade and Industry, Her Majesty's Stationary Office (London), 1971.

16. Huffman, G. David: Theory, Performance, and Design of Flow Direction and Mach
    Number Probes. AFATL TR-81-44, U.S. Air Force Armament Laboratory, 1981.

17. Gallington, Roger W.: Measurement of Very Large Flow Angles With Non-Nulling
    Seven-Hole Probes. 27th ISA Symposium Proc., part 1, 1981, pp. 115-130.

18. Larson, Terry, J.: Compensated and Uncompensated Nose Boom Static Pres-
    sures Measured From Two Air Data Systems on a Supersonic Airplane. NASA
    TM X-3132, 1974.

19. Gilyard, Glenn B.; and Belte, Daumants: Flight-Determined Lag of Angle-of-
    Attack and Angle-of-Sideslip Sensors in the YF-12A Airplane From Analysis
    of Dynamic Maneuvers. NASA TN D-7819, 1974.

20. Gracey, William: Wind-Tunnel Investigation of a Number of Total-Pressure Tubes
    at High Angles of Attack: Subsonic, Transonic, and Supersonic Speeds. NACA
    Report 1303, 1957.

21. Armistead, Katharine H.; and Webb, Lannie D.: Flight Calibration Tests of
    a Nose-Boom-Mounted Fixed Hemispherical Flow-Direction Sensor. NASA
    TN D-7461, 1973.

22. Larson, Terry J.; and Ehernberger, L.J.: Techniques Used for Determination of
    Static Source Position Error of a High-Altitude Supersonic Airplane. NASA
    TM X-3152, 1975.

23. Larson, Terry J.; and Ehernberger, L.J.: A Constant Altitude Flight Survey
    Method for Mapping Atmospheric Ambient Pressures and Systematic Radar Errors.
    NASA TM-86733, 1985.

24. Etkin, B.: Dynamics of Flight. John Wiley & Sons, Inc., New York, 1959.

25. Eykhoff, P.: System Identification. John Wiley & Sons, Inc., New York, 1974.

26. U.S. Standard Atmosphere, 1976. NOAA-S/T 76-1562, NOAA, NASA, and
    U.S. Air Force, 1976.

TABLE 1. — MAXIMUM UNCERTAINTIES AND RESOLUTIONS OF RECORDED MEASUREMENTS

Measurement	Uncertainty	Resolution	Measurement	Uncertainty	Resolution
a_n, g	±0.02	0.011	P_{16}, N/cm^2	±0.0100	0.0040
a_x, g	±0.02	0.006	P_{17}, N/cm^2	±0.0100	0.0040
a_y, g	±0.02	0.006	P_{18}, N/cm^2	±0.0050	0.0020
P_{IR}, N/cm^2	±0.0014	0.0005	P_{19}, N/cm^2	±0.0100	0.0010
$(P_t)_{IR}$, N/cm^2	±0.0014	0.0120	P_{20}, N/cm^2	±0.0130	0.0010
P_2, N/cm^2	±0.0220	0.0210	P_{21}, N/cm^2	±0.0130	0.0050
P_3, N/cm^2	±0.0220	0.0210	P_{22}, N/cm^2	±0.0014	0.0005
P_4, N/cm^2	±0.0014	0.0005	P_{23}, N/cm^2	±0.0130	0.0050
P_5, N/cm^2	±0.0080	0.0070	P_{24}, N/cm^2	±0.0130	0.0050
P_6, N/cm^2	±0.0080	0.0070	P_{25}, N/cm^2	±0.0130	0.0060
P_7, N/cm^2	±0.0080	0.0070	P_{26}, N/cm^2	±0.0100	0.0040
$P_{8,11}$, N/cm^2	±0.0210	0.0200	P_{27}, N/cm^2	±0.0140	0.0050
$P_{9,10}$, N/cm^2	±0.0210	0.0200	p, deg/sec	±0.6	0.05
P_{12}, N/cm^2	±0.0150	0.0060	q, deg/sec	±1.20	0.07
P_{13}, N/cm^2	±0.0070	0.0030	r, deg/sec	±0.6	0.05
P_{14}, N/cm^2	±0.0100	0.0040	α, deg	±0.1	0.1
P_{15}, N/cm^2	±0.0150	0.0030	β, deg	±0.1	0.1
			φ, deg	±2.0	0.2

TABLE 2. — FADS FLIGHT TEST CONDITIONS

Maneuver	h_p, km	Mach
Constant h_p and Mach survey	3.3	0.80
Sideslip in trim	3.3	0.90
Sideslip at high angle of attack	3.3	0.90
Angle-of-attack	3.3	0.95
Angle-of-attack	3.3	1.05
Acceleration-deceleration	13.1	0.60 to 1.40
Angle-of-attack	13.1	1.20
Constant h_p and Mach survey	13.1	0.80
Angle-of-attack	11.5	0.90
Sideslip in trim	11.5	0.90
Sideslip in trim	11.5	0.90
Angle-of-attack	9.8	0.60
Sideslip at high angle of attack	9.8	0.60
Stabilized, pacer	9.8	0.60
Stabilized, pacer	9.8	0.65
Stabilized, pacer	9.8	0.70
Stabilized, pacer	9.8	0.75
Stabilized, pacer	9.8	0.80
Stabilized, pacer	9.8	0.85
Stabilized, pacer	9.8	0.90
Acceleration-deceleration	11.5	0.60 to 1.50
Constant h_p and Mach survey	11.5	0.80
Angle-of-attack	9.8	0.80
Sideslip in trim	9.8	0.80
Sideslip at high angle of attack	9.8	0.90
Angle-of-attack	11.5	0.90
Sideslip in trim	11.5	0.90
Sideslip at high angle of attack	11.5	0.90

TABLE 3. — OPTIMUM ORIFICES FOR AIR DATA MEASUREMENTS

Air data measurement	Orifice location			
	Nose cap	Station		Best overall
		61	127	
Mach	3,7			3,7
P_t	4			4
p		12,14	16,20	12,14
α	3,7	12,14	16,20	3,7
β	8,11	13,15	18,22	8,11

TABLE 4. — AIR DATA SENSITIVITY TO ALTIMETRY ERROR

Flight condition		Increment due to 0.1-percent ambient pressure change		
h_p, km	Mach	Δh_p, m	ΔM	ΔV, knots
Sea level	0.50	8.39	0.0015	1.70
Sea level	1.14	8.39	0.0008	0.90
12.192	0.80	6.34	0.0010	1.00
12.192	1.14	6.34	0.0008	0.80
12.192	2.50	6.34	0.0013	1.45
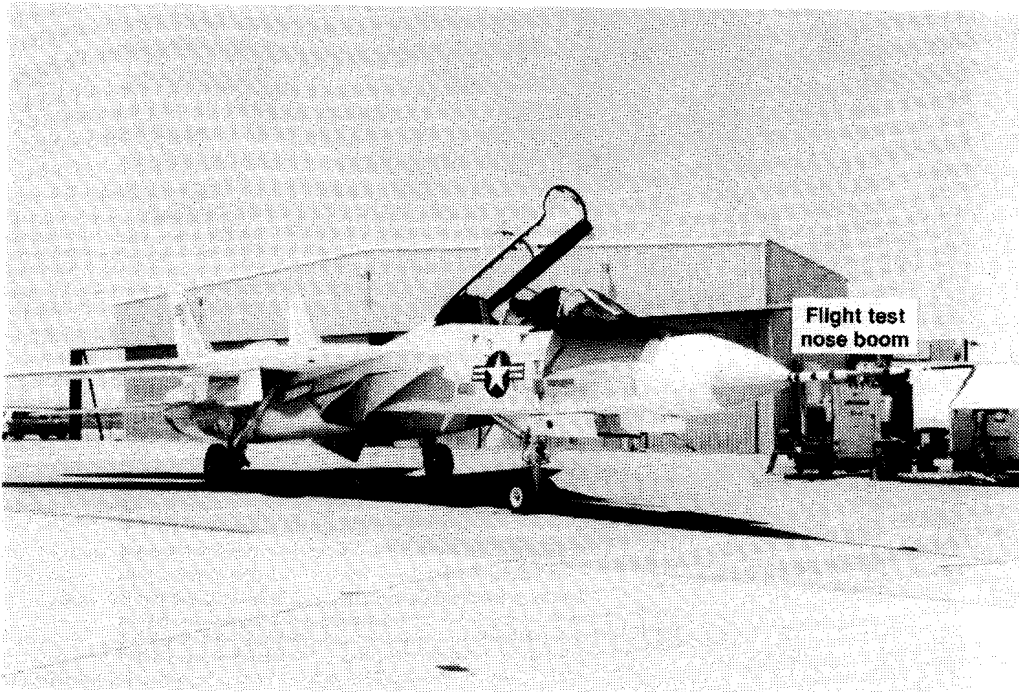
ECN 12745

Figure 1. F-14 airplane with flight test nose boom.
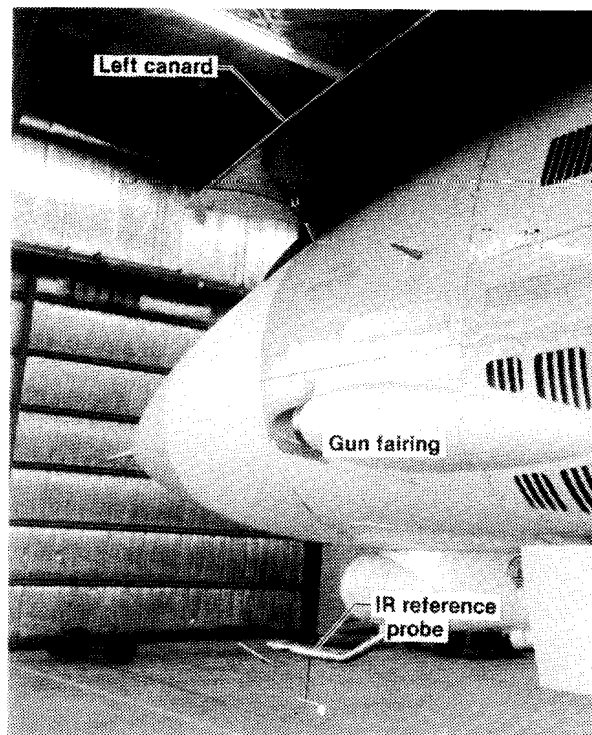
E 39381

Figure 2. Forebody of test aircraft.
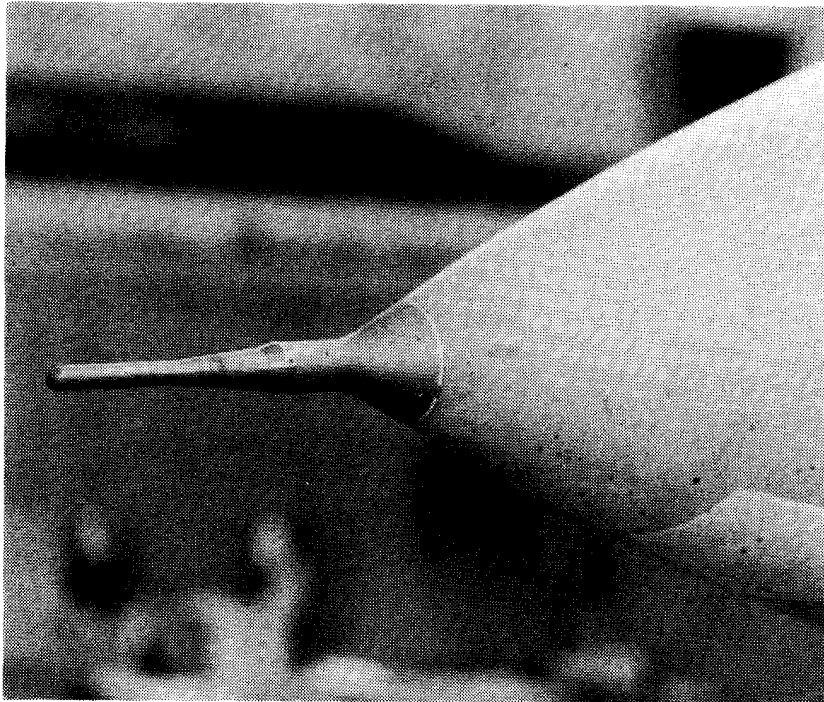
E 39384

Figure 3. Hemispherical flow direction probe.
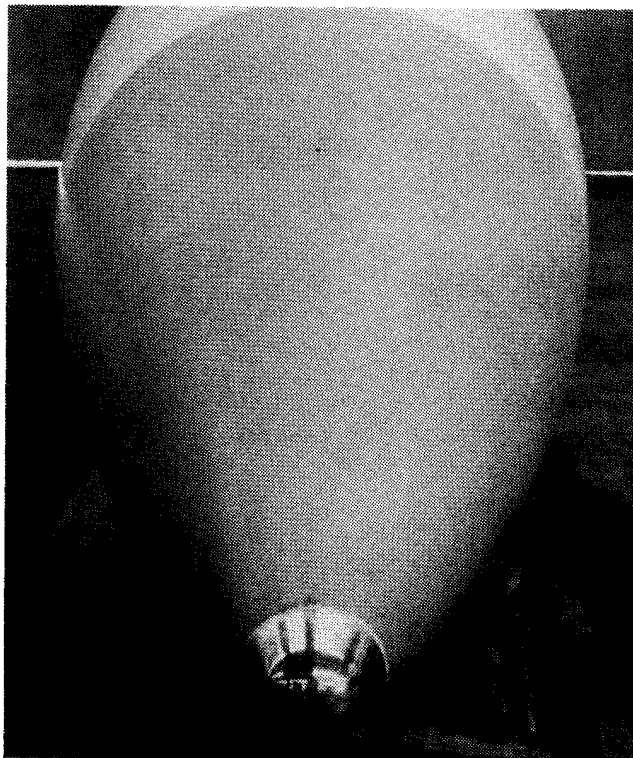
ECN 22769

Figure 4. FADS nose cap blended with F-14 nose cone.

Orifices 1 to 7 are spaced
in increments of 20°
Orifices 8 to 11 are spaced
in increments of 30°
All orifices are 0.08 cm in
diameter

4.19-cm radius

60°

Aircraft
longitudinal
axis

5°

Side view

Front view
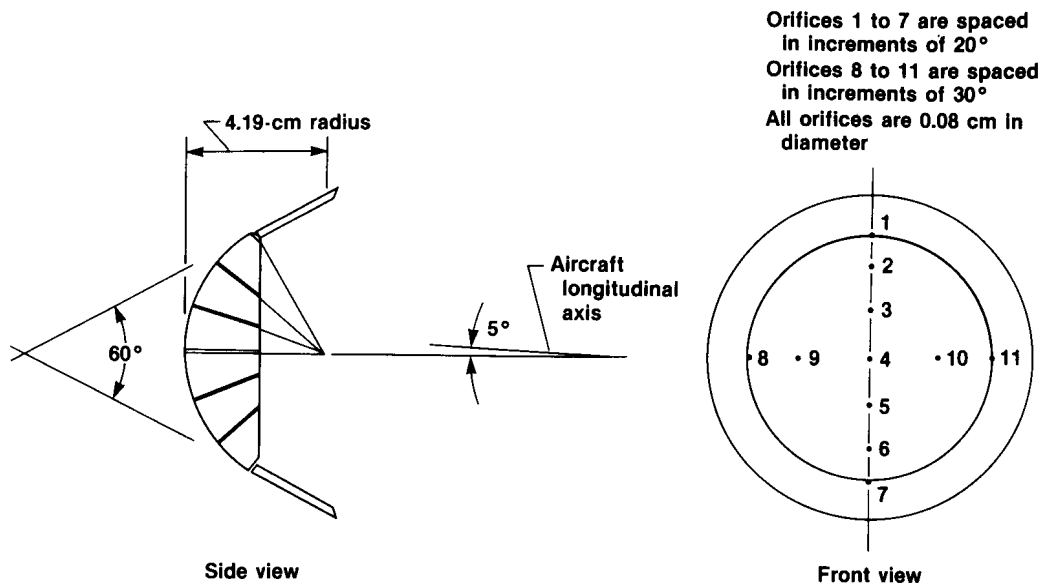
Figure 5. Sectional views of FADS nose cap.

All orifices are 0.318 cm in
diameter
Rows are normal to fuselage
longitudinal axis
Station 61 orifices are on vertical
and horizontal centerlines
Station 127 orifices are spaced
either 15° or 45° apart

Station 61

Station 127

IR scanner pod

Station 61

Station 127
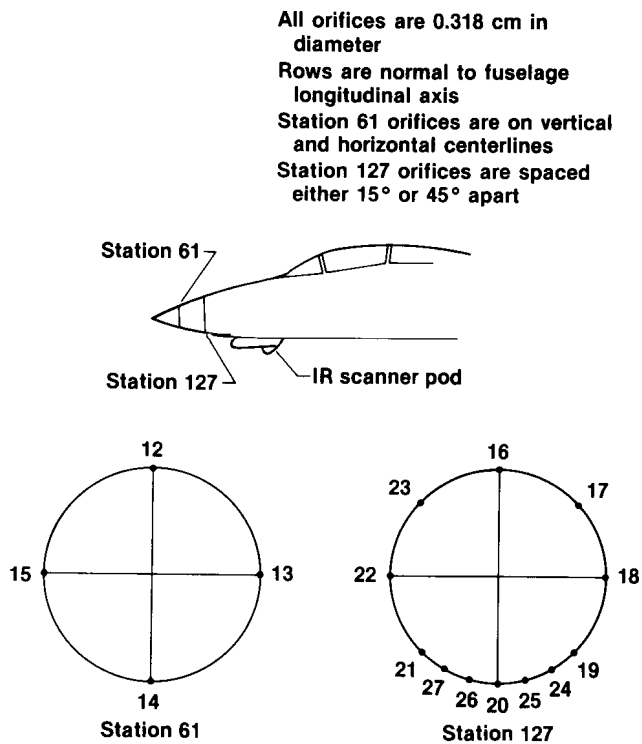
*Figure 6. Nose section pressure ori-
fices (numbered locations as viewed
from front of nose cone).*

29
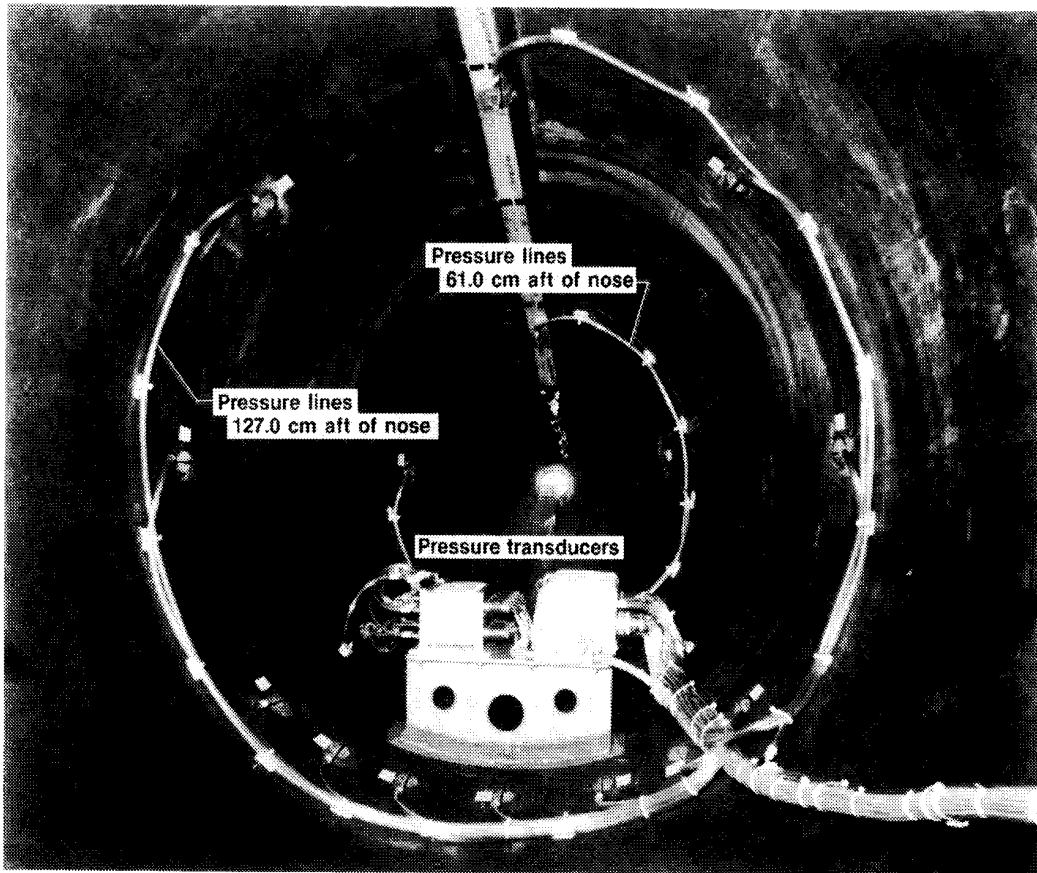
ECN 22770

Figure 7. Pressure lines and transducers (looking forward inside nose cone).
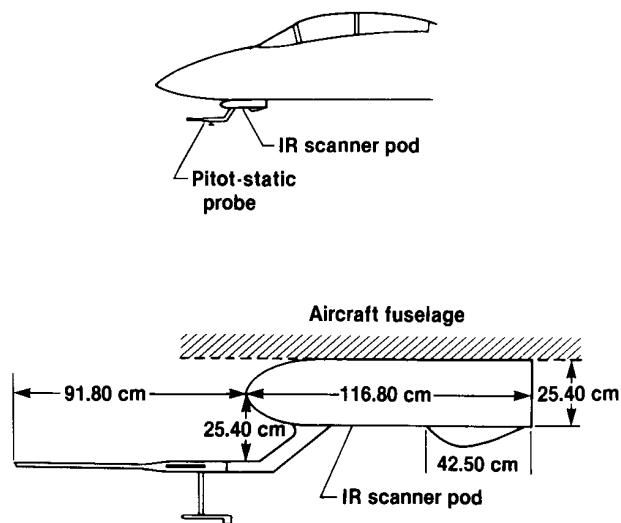
Figure 8. Standard NASA pitot-static probe (ref. 12) installed on IR pod.

Method

- ○ Radar, decreasing Mach
- □ Radar, increasing Mach
- ◇ Pacer
- △ LKF reconstruction
- — Calibration curve

$\Delta M = M - M_i$
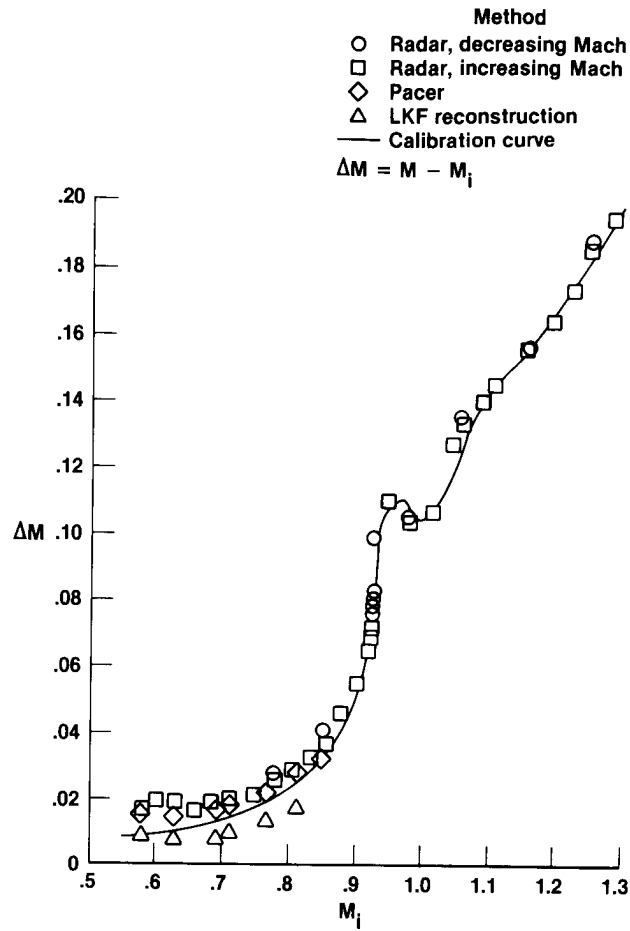
Figure 9. Comparison of IR probe calibration data (nose boom removed) with calibration curve (nose boom on), $\alpha < 6.0°$.

(a) *Mach.*

(b) *Pressure altitude.*
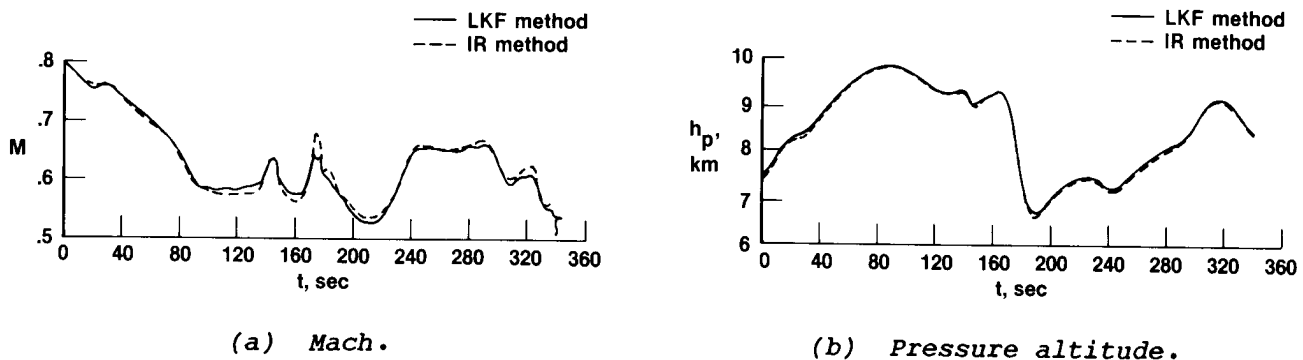
Figure 10. Comparison of LKF trajectory quantities with those measured by IR reference probe and determined from upper air analysis.
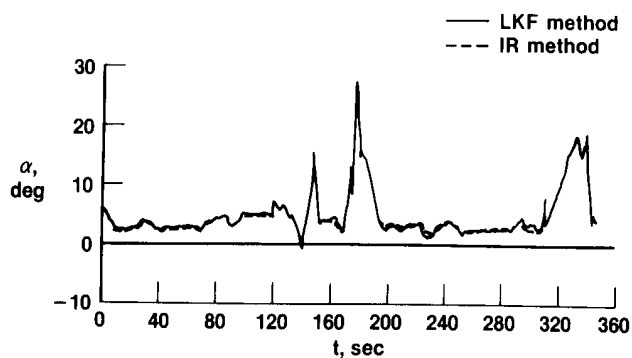
(c) Angle of attack.
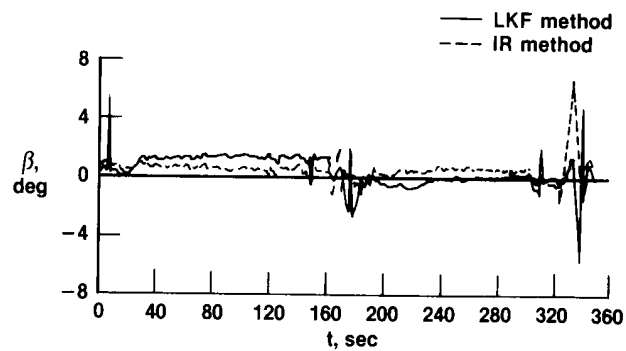
(d) Angle of sideslip.
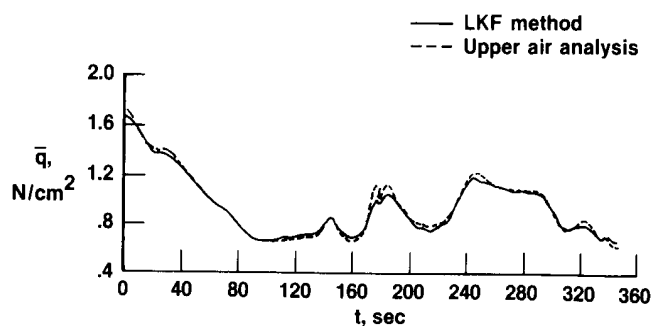
(e) Dynamic pressure.
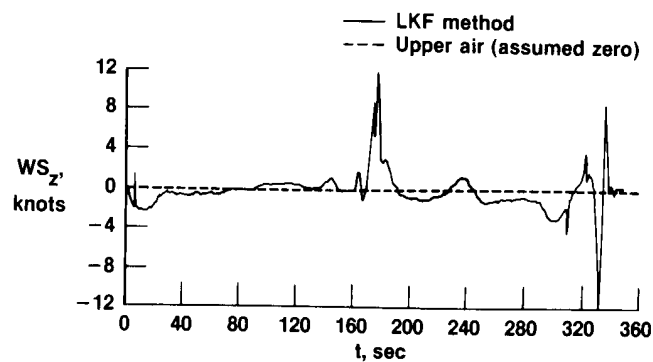
(f) Vertical windspeed.
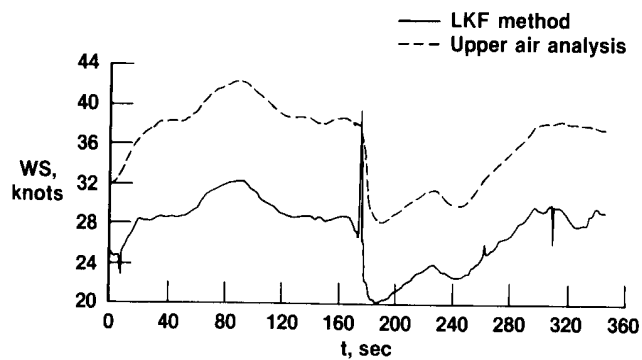
(g) Windspeed.
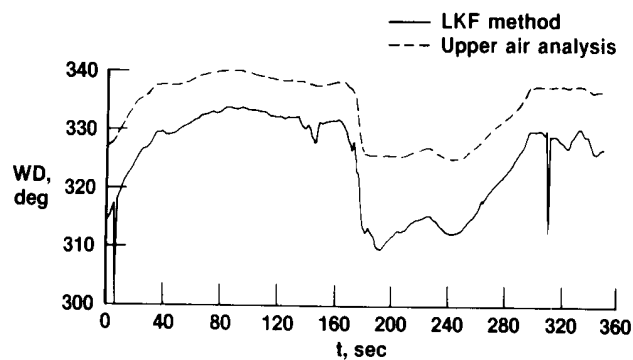
(h) Wind direction.

Figure 10. Concluded.
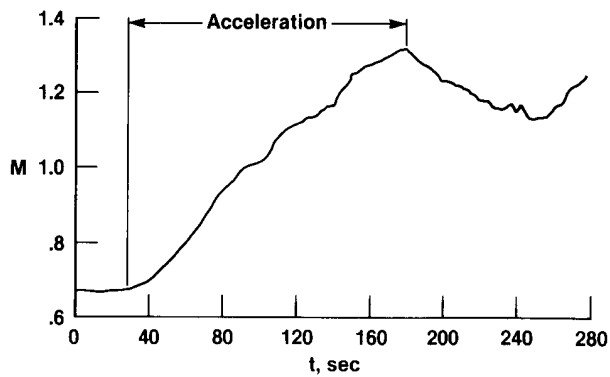
(a) Reference Mach.
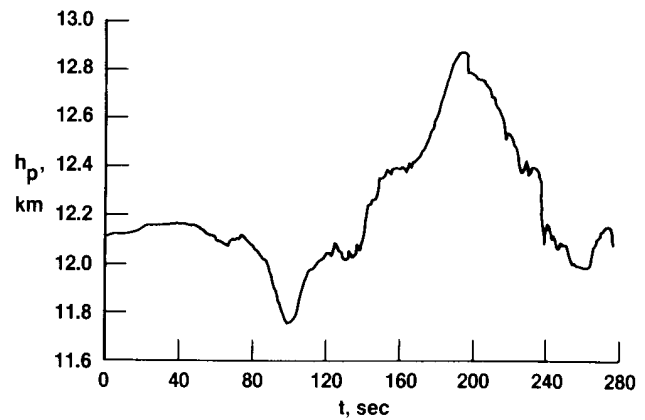
(b) Reference pressure altitude.
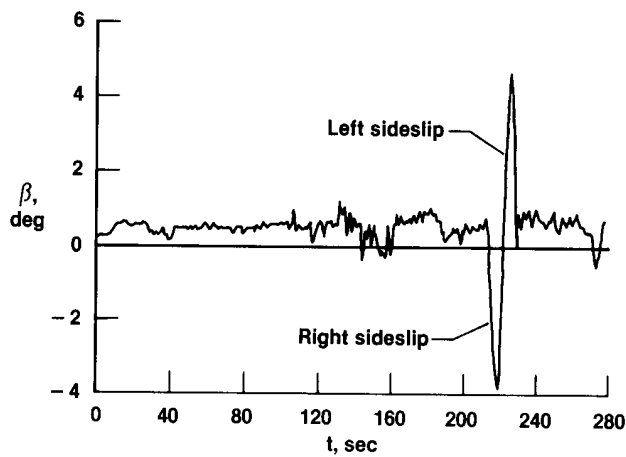
(c) Reference angle of sideslip.
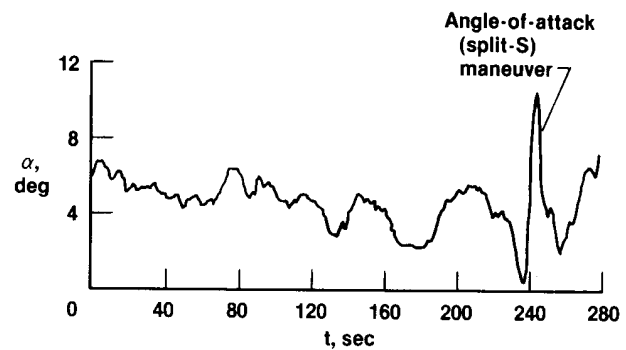
(d) Reference angle of attack.
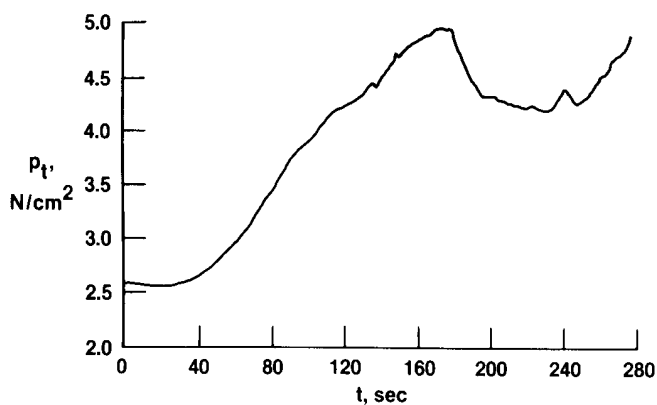
(e) Reference stagnation pressure.
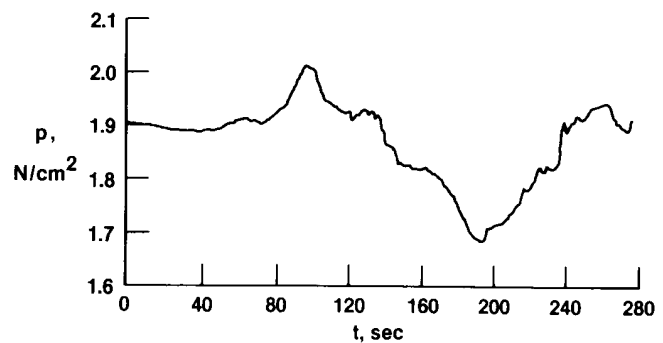
(f) Reference static pressure.

Figure 11. Time histories of reference conditions and FADS pressures during maneuvering flight tests.
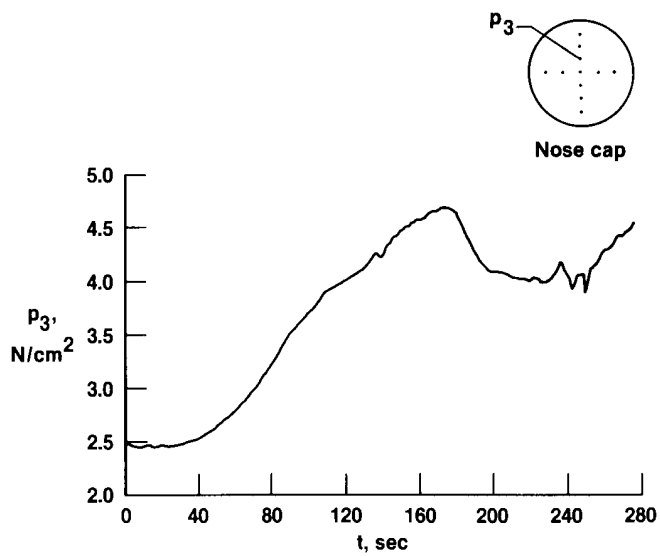
(g)   Pressure measured at orifice 3.
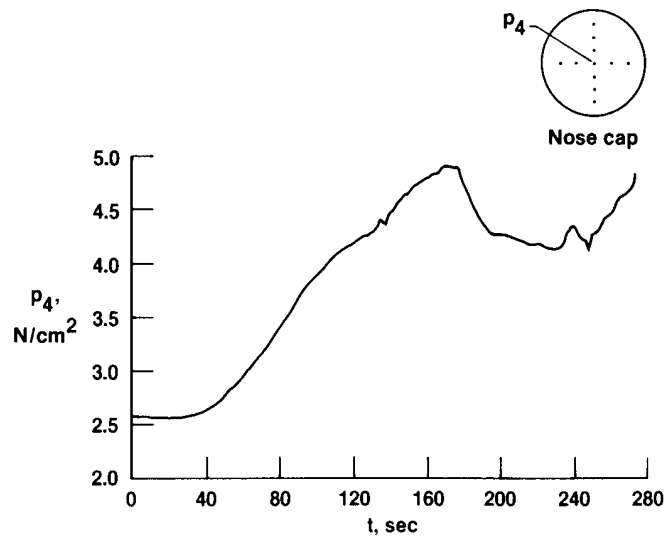
(h)   Pressure measured at orifice 4.
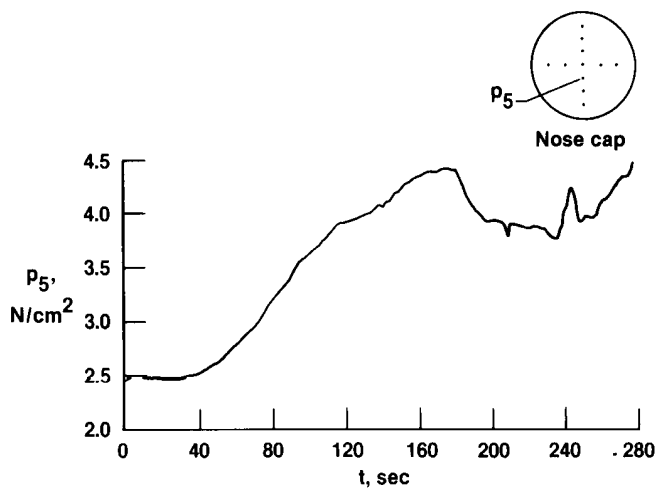
(i)   Pressure measured at orifice 5.
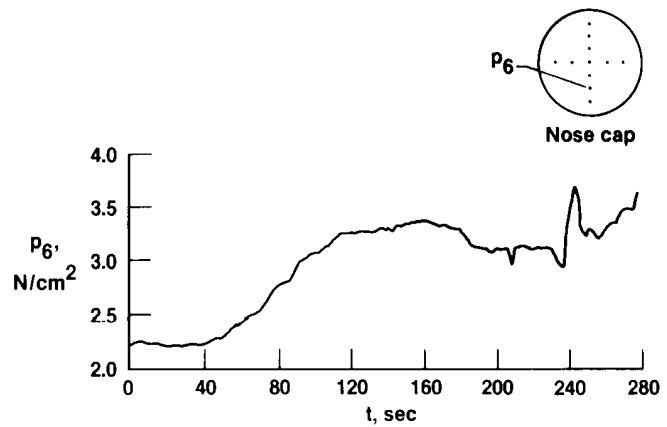
(j)   Pressure measured at orifice 6.

Figure 11.   Continued.
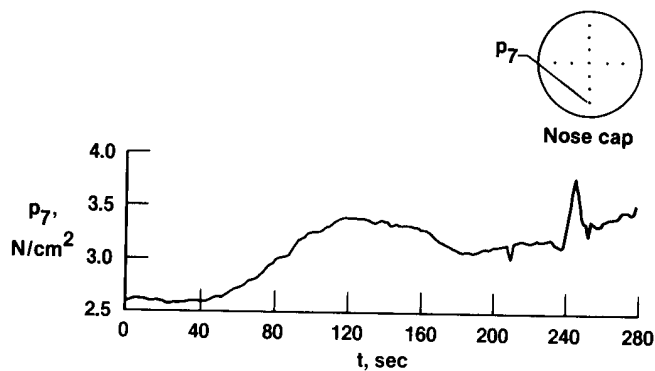
(k) Pressure measured at orifice 7.
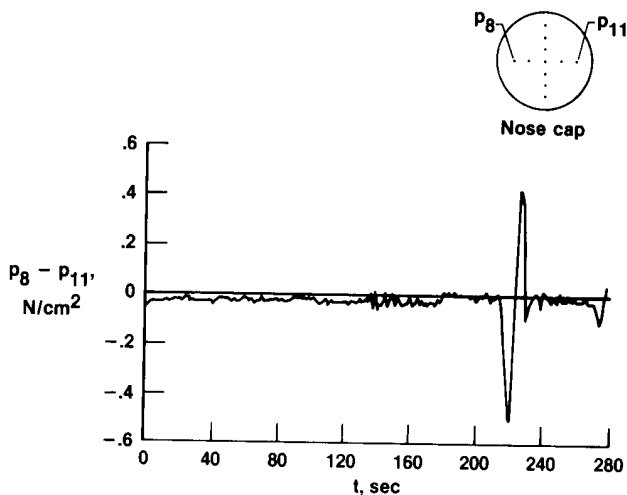
(l) Differential pressure measured between orifices 8 and 11.
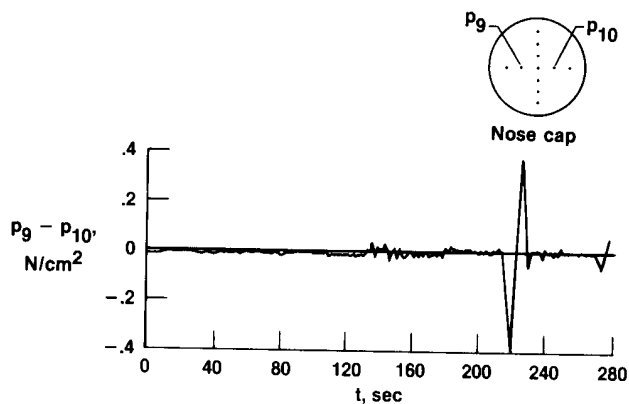
(m) Differential pressure measured between orifices 9 and 10.
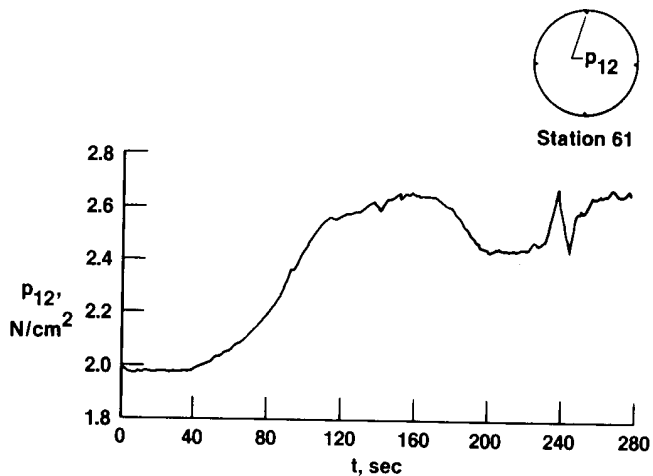
(n) Pressure measured at orifice 12.

Figure 11. Continued.
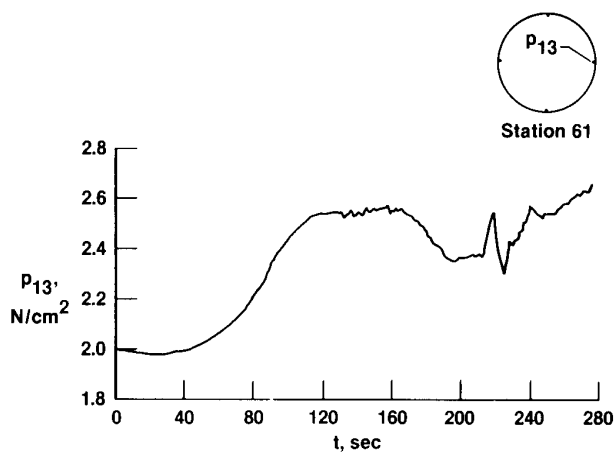
(o) Pressure measured at orifice 13.
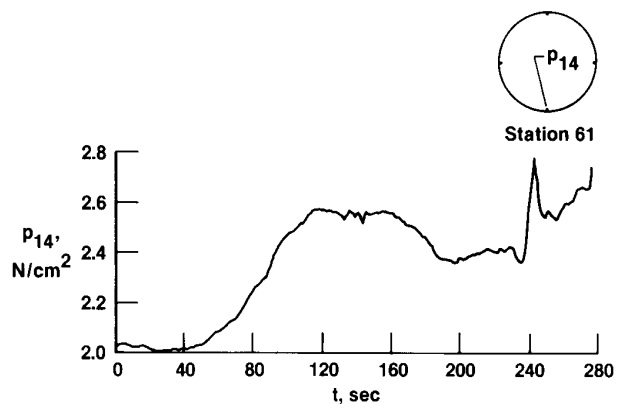
(p) Pressure measured at orifice 14.
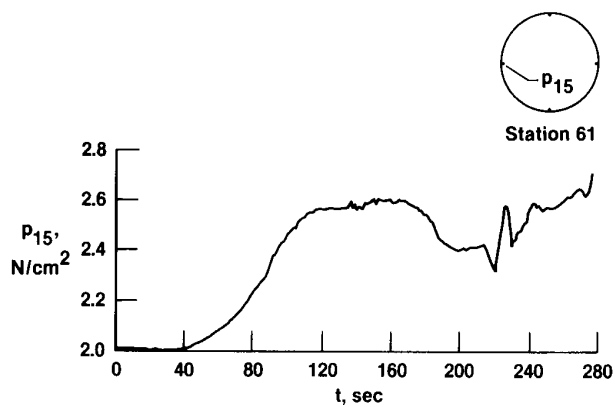
(q) Pressure measured at orifice 15.
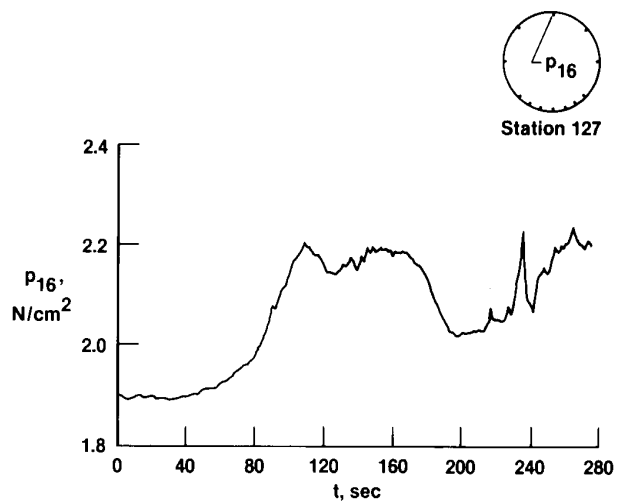
(r) Pressure measured at orifice 16.

Figure 11. Continued.
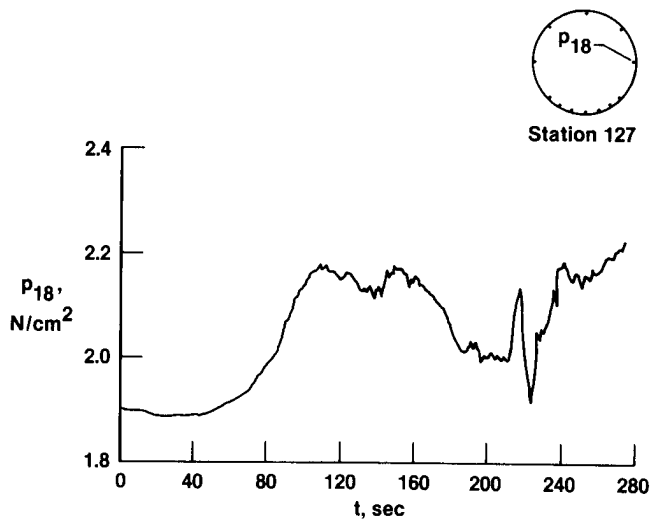
(s) *Pressure measured at orifice 18.*
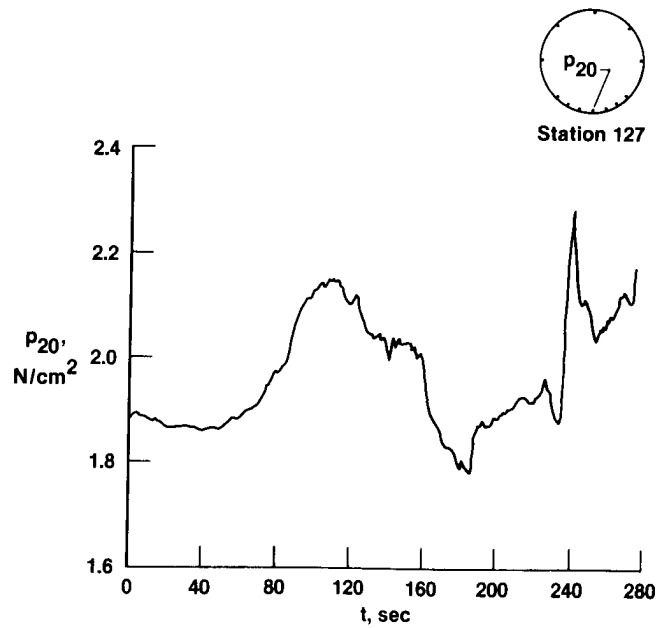
(t) *Pressure measured at orifice 20.*
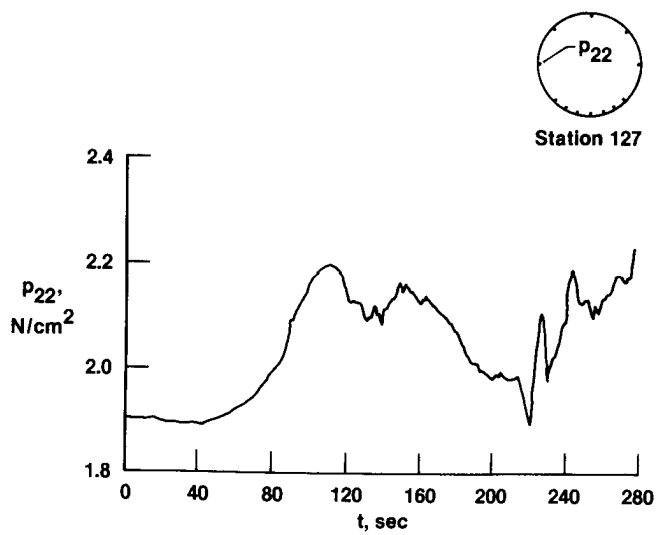
(u) *Pressure measured at orifice 22.*

Figure 11. Concluded.

37
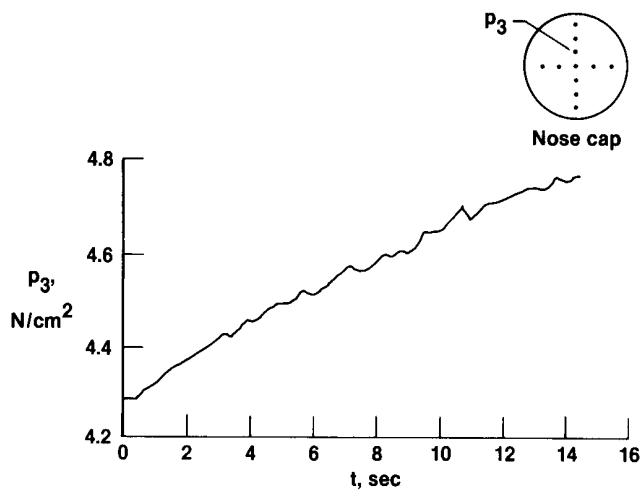
(a) Pressure measured at orifice 3.
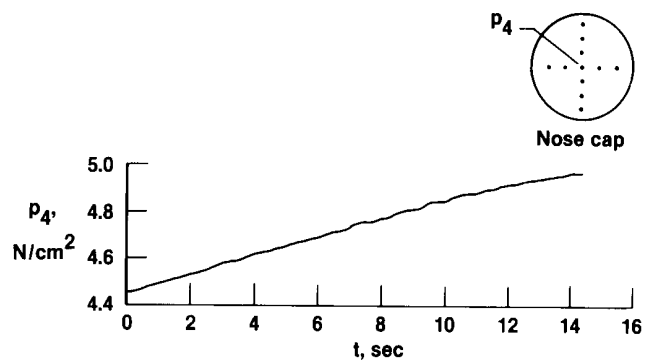
(b) Pressure measured at orifice 4.
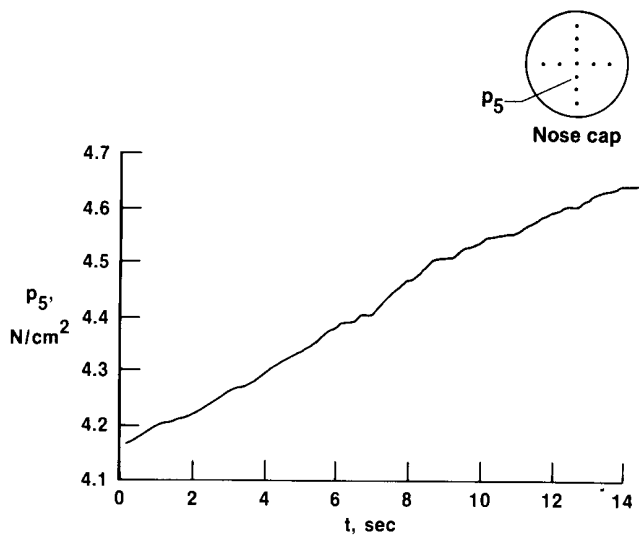
(c) Pressure measured at orifice 5.
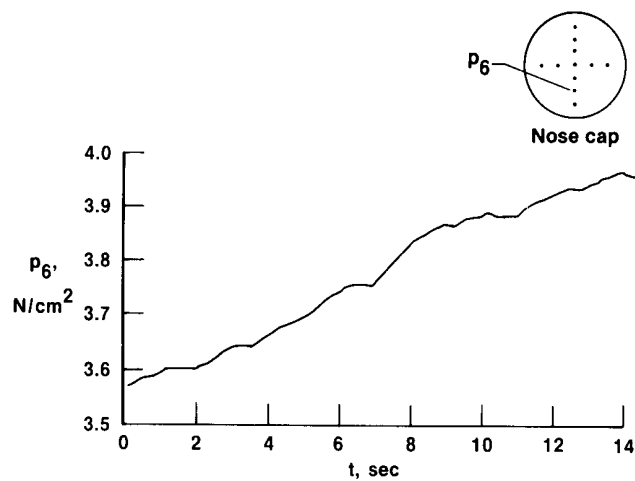
(d) Pressure measured at orifice 6.

Figure 12. Time histories of FADS nose cap pressures during acceleration to sonic speeds from M = 0.98 to 1.04.
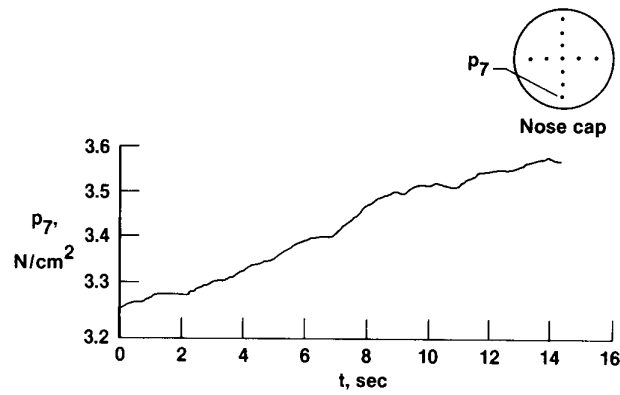
(e)   Pressure measured at orifice 7.

Figure 12.   Concluded.
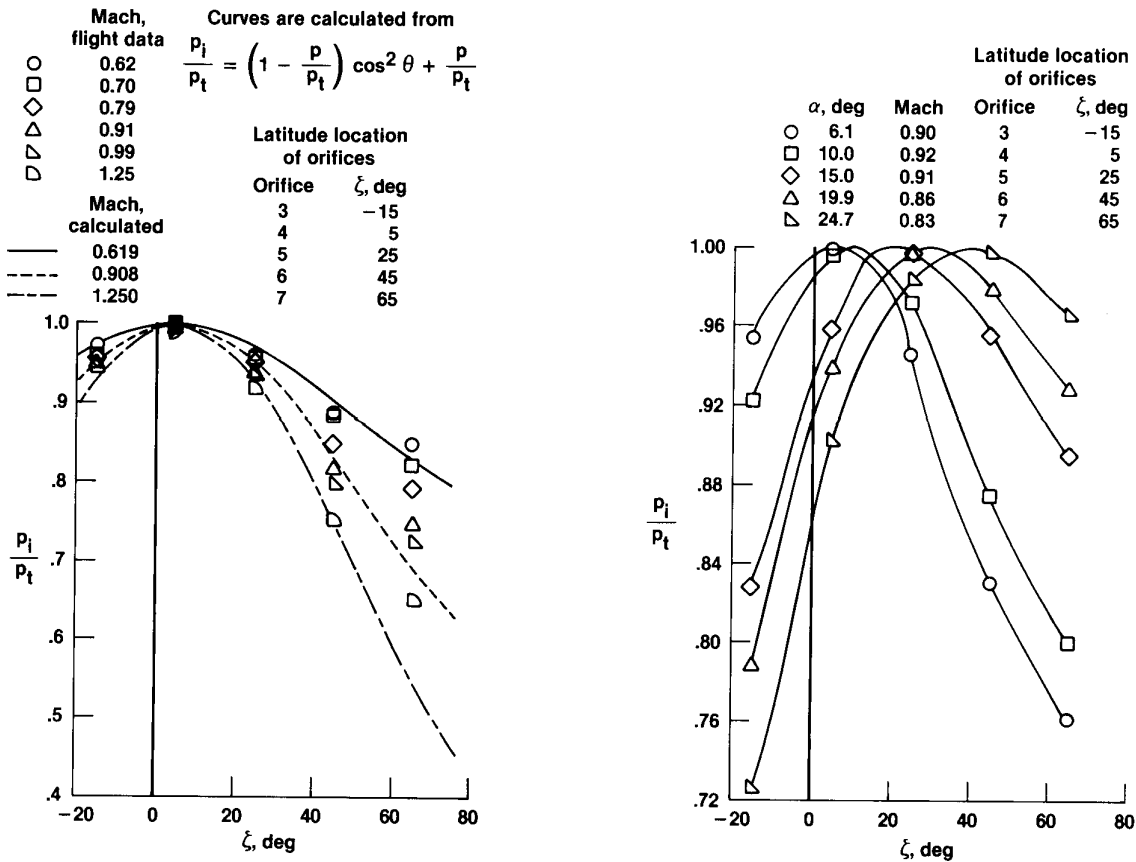
(a)   Effect of Mach, $\alpha = 5.0°$.

(b)   Effect of angle of attack.

Figure 13.   Pressure distribution on nose cap predicted by modified Newtonian flow compared with measured data.

$$PTP_{14} = \frac{p_4}{p_t}$$

$$PTP_{15} = \frac{p_5}{p_t}$$

$$PTP_{16} = \frac{p_6}{p_t}$$

○ Decreasing α
□ Increasing α

Nose cap
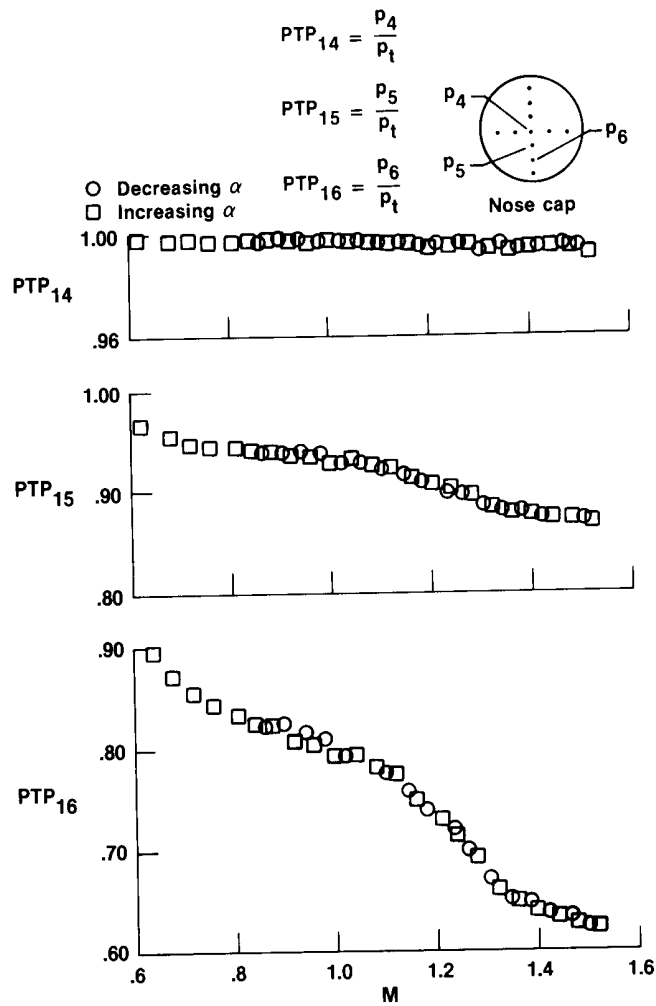
Figure 14. Stagnation pressure parameter as a function of Mach, $\alpha = 0.0°$ *to 5.9°.*

$$PTP_{14} = \frac{p_4}{p_t}$$

First flight
○ Decreasing α $\quad PTP_{15} = \dfrac{p_5}{p_t}$
□ Increasing α
Second flight
◇ Decreasing α $\quad PTP_{16} = \dfrac{p_6}{p_t}$
△ Increasing α

Nose cap

(a) $M = 0.57$ to 0.68.

$$PTP_{14} = \frac{p_4}{p_t}$$

First flight
○ Decreasing α $\quad PTP_{15} = \dfrac{p_5}{p_t}$
□ Increasing α
Second flight
◇ Decreasing α $\quad PTP_{16} = \dfrac{p_6}{p_t}$
△ Increasing α

Nose cap

(b) $M = 0.87$ to 0.92.

$$PTP_{14} = \frac{p_4}{p_t}$$

$$PTP_{15} = \frac{p_5}{p_t}$$

○ Decreasing α $\quad PTP_{16} = \dfrac{p_6}{p_t}$
□ Increasing α

Nose cap
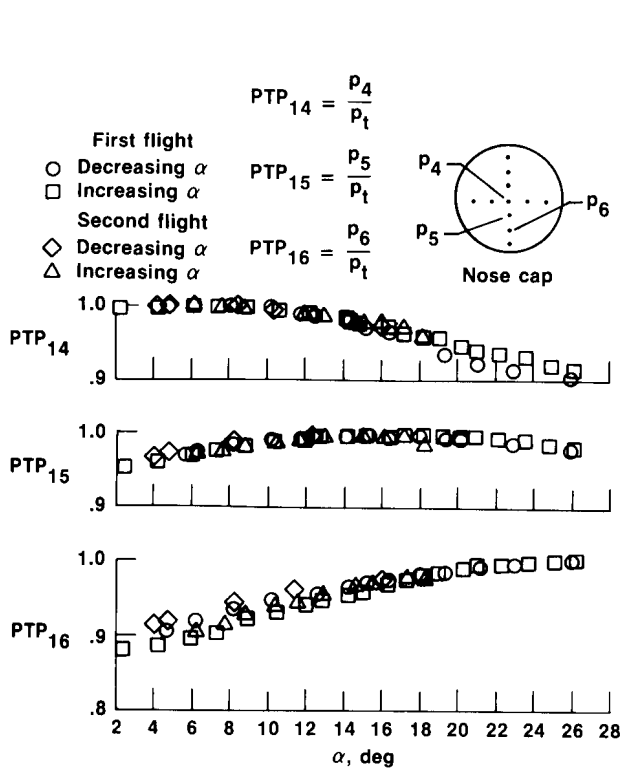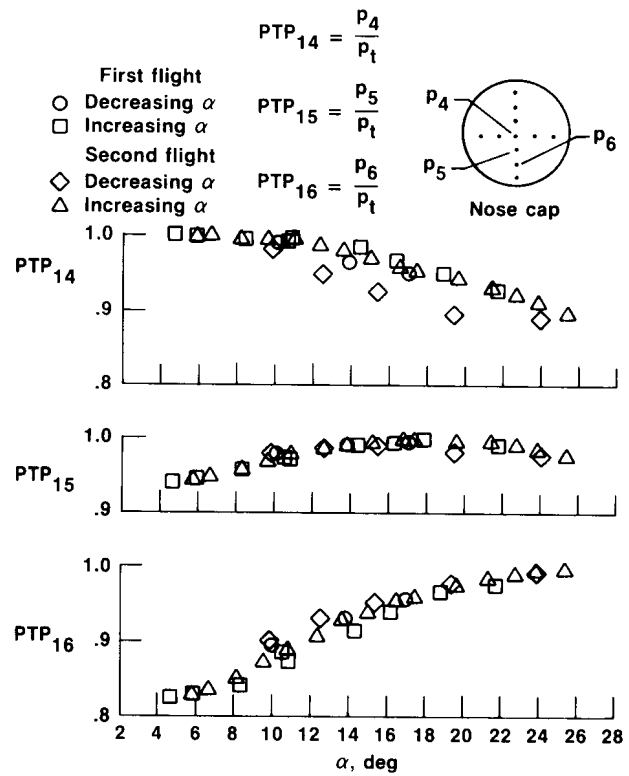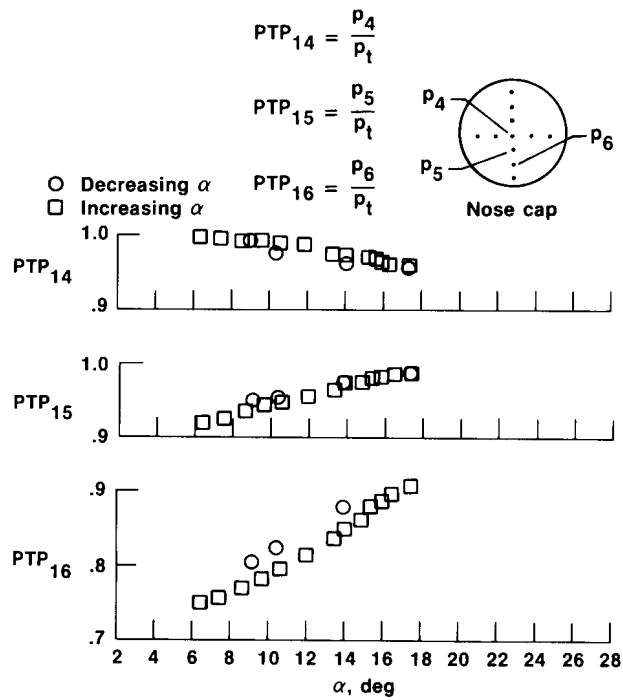
(c) $M = 1.21$ to 1.25.

Figure 15. Stagnation pressure parameter as a function of angle of attack.

41

$$PTP_{14} = \frac{P_4}{P_t}$$

$$PTP_{15} = \frac{P_5}{P_t}$$

$$PTP_{16} = \frac{P_6}{P_t}$$
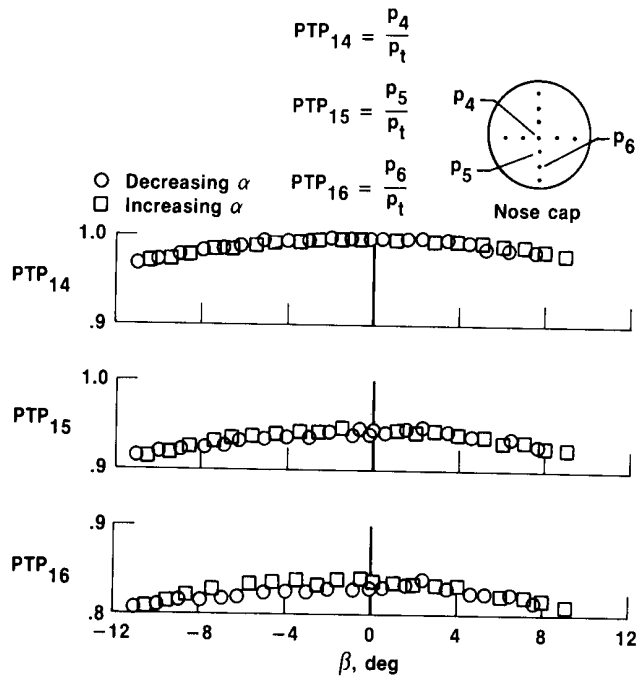
(a) *M = 0.75 to 0.80.*
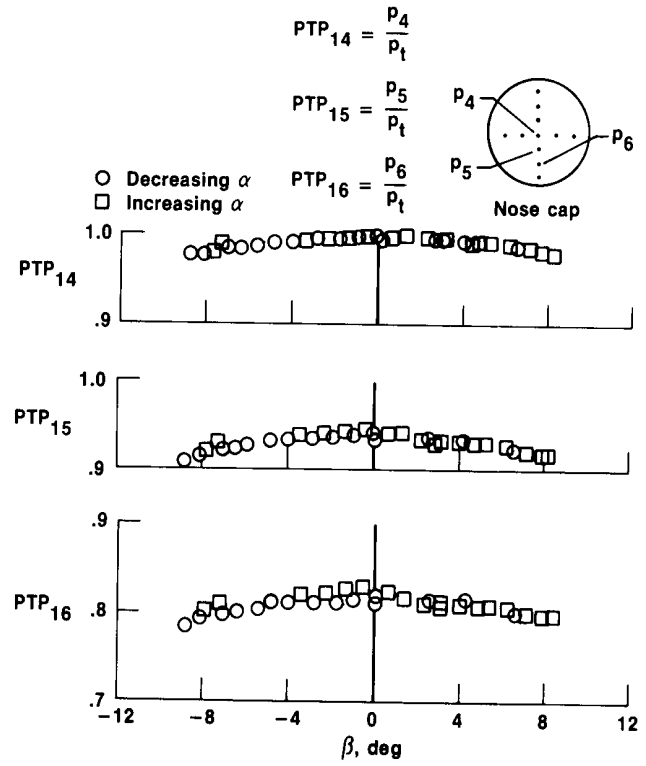
(b) *M = 0.87 to 0.92.*

Figure 16. Stagnation pressure parameter as a function of angle of sideslip,
α = 1.8° to 5.6°.

$$PP_{22} = \frac{p_{12} + p_{14}}{2p}$$

○ Decreasing α
□ Increasing α

Station 61

$$PP_{32} = \frac{p_{16} + p_{20}}{2p}$$

$$PP_{3ALL} = \frac{p_{16} + \ldots + p_{27}}{12p}$$

○ Decreasing α
□ Increasing α
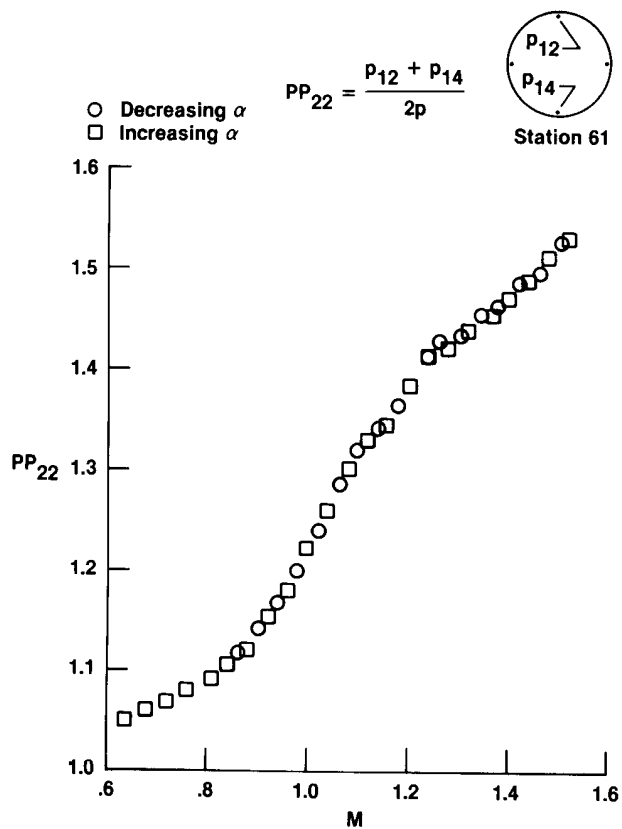
Station 127

(a) *Orifices at station 61.*
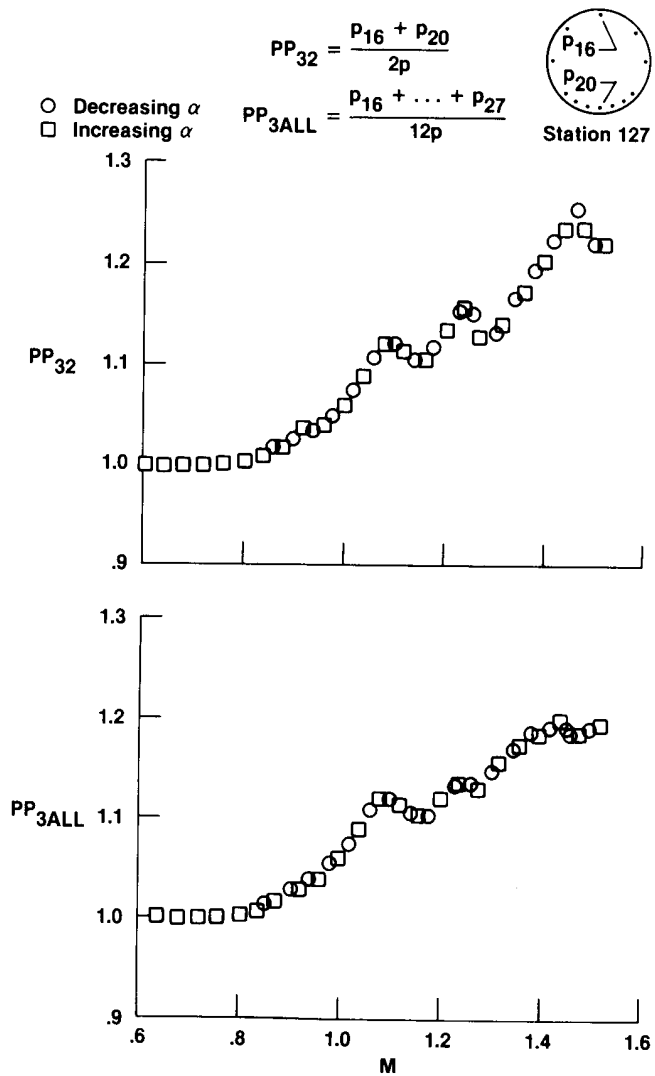
(b) *Orifices at station 127.*

Figure 17. *Static pressure parameter as a function of Mach.*
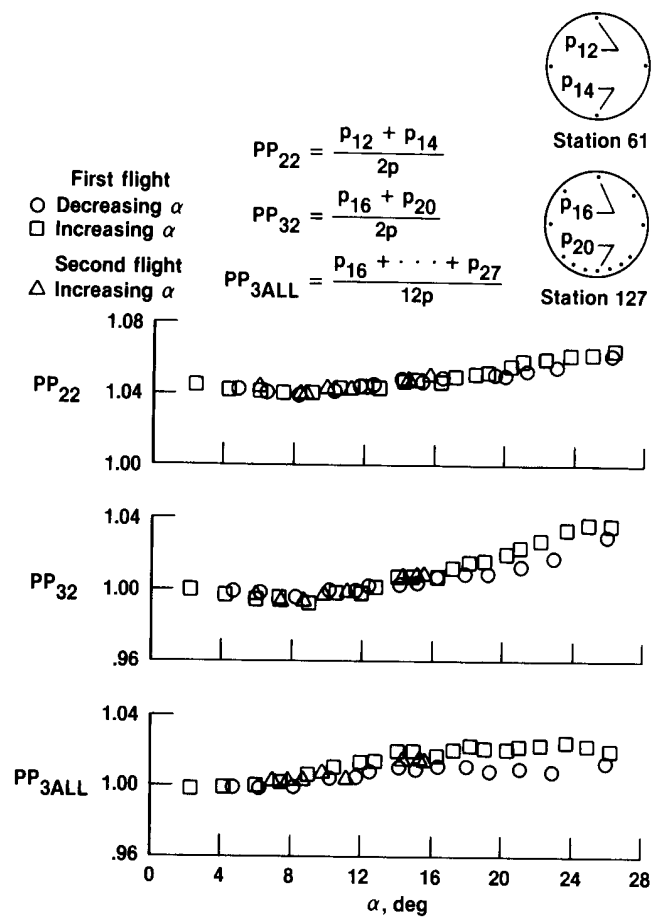
(a) Mach corrected to M = 0.60 (M = 0.57 to 0.68, actual range).
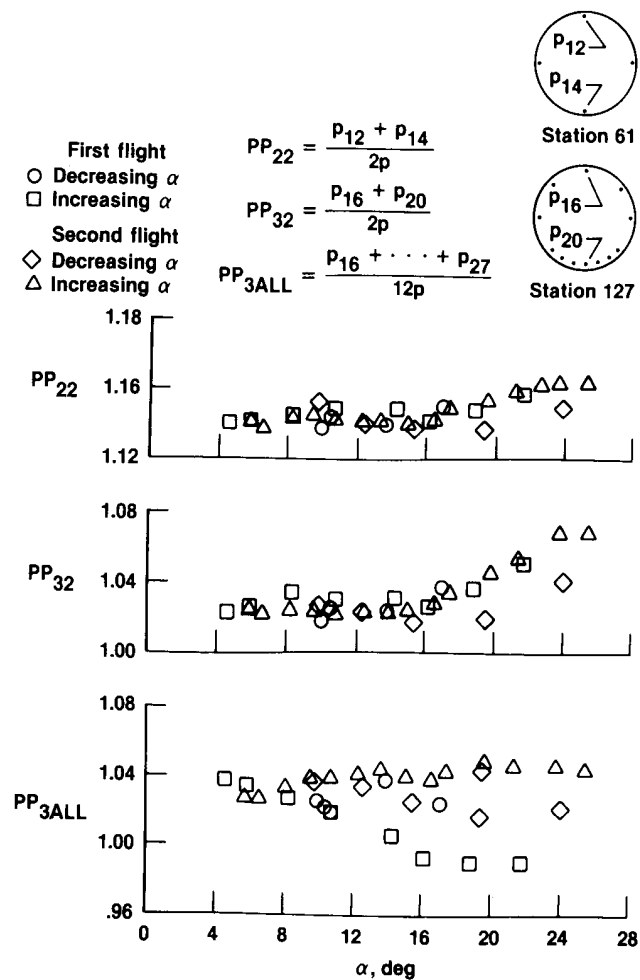
(b) Mach corrected to M = 0.90 (M = 0.79 to 0.96, actual range).

Figure 18. Static pressure parameter as a function of angle of attack.
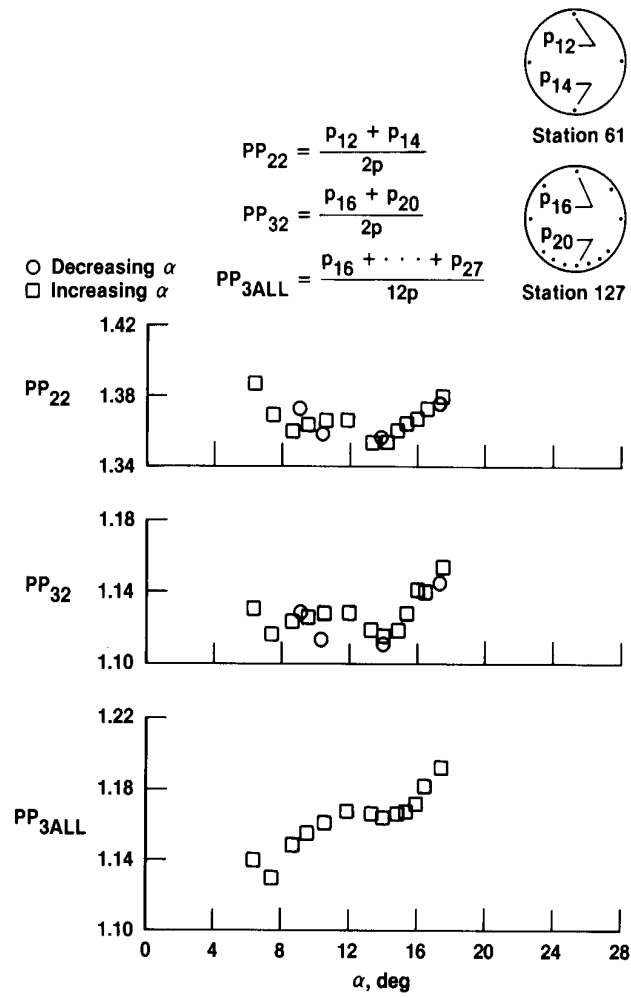
(c) Mach corrected to M = 1.23 (M = 1.21
to 1.26, actual range).

Figure 18. Concluded.

$$PP_{22} = \frac{p_{12} + p_{14}}{2p}$$

$$PP_{32} = \frac{p_{16} + p_{20}}{2p}$$

$$PP_{3ALL} = \frac{p_{16} + \cdots + p_{27}}{12p}$$
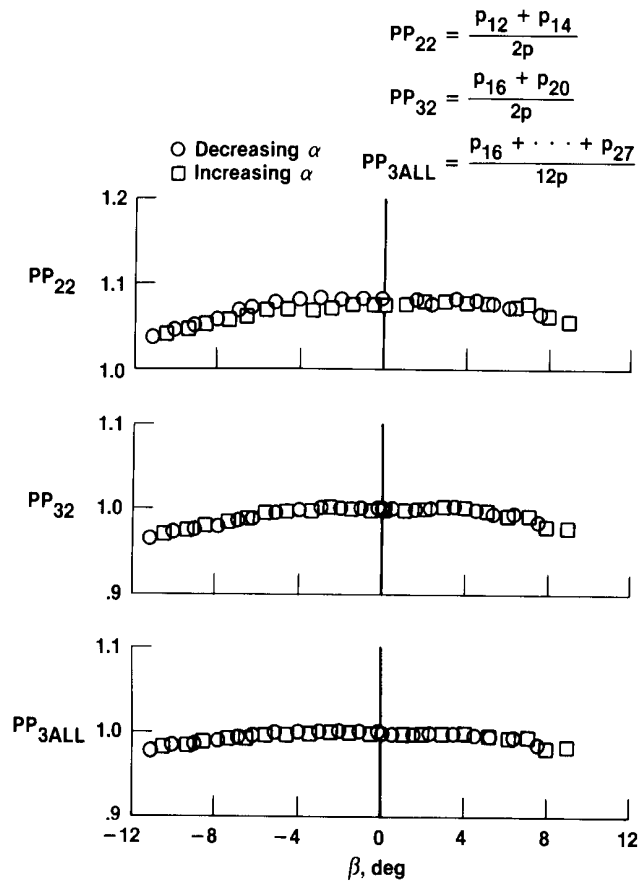
(a) *M = 0.75 to 0.80.*
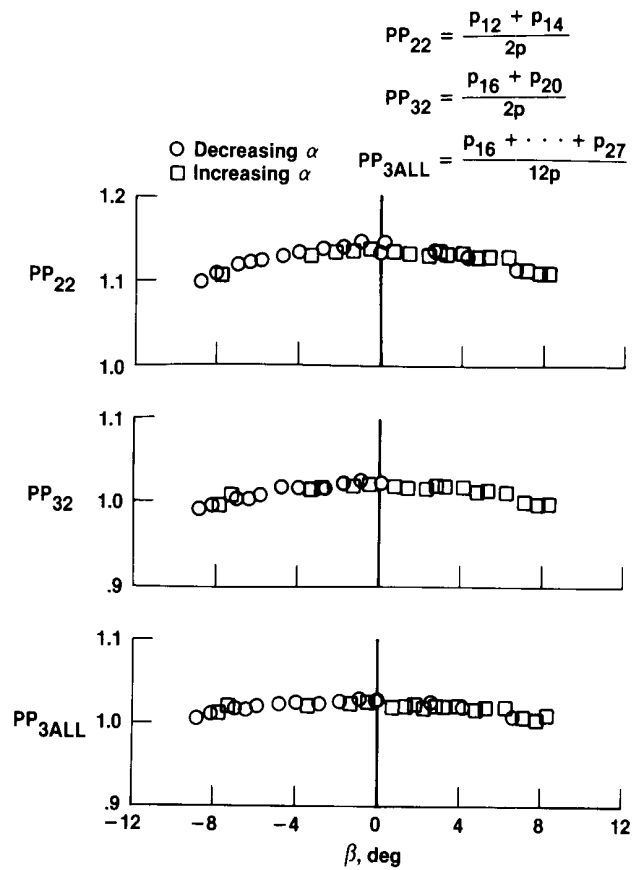
(b) *M = 0.87 to 0.92.*

Figure 19. Static pressure parameter as a function of angle of sideslip, α = 1.8° to 5.6°.
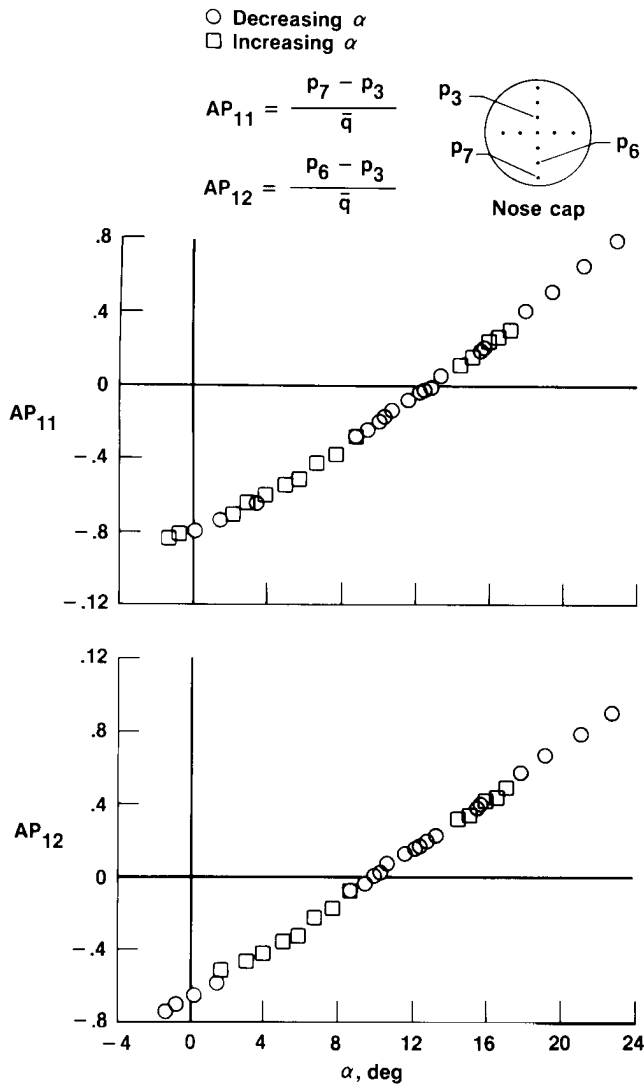
(a) *M = 0.60, orifices on nose cap.* (b) *M = 0.60, orifices at station 61.*
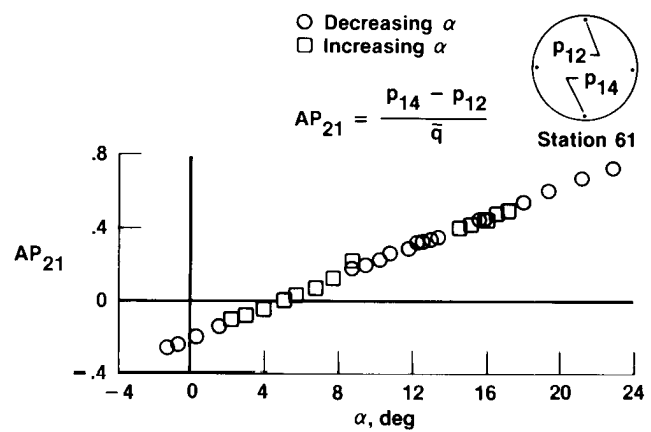
Figure 20. *Angle-of-attack parameter as a function of angle of attack.*
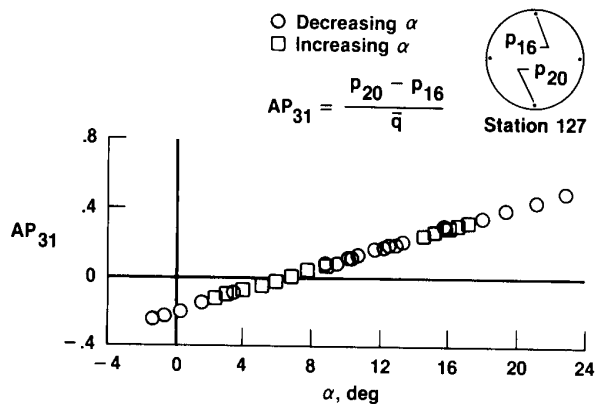
(c) *M = 0.60, orifices at station 127.*
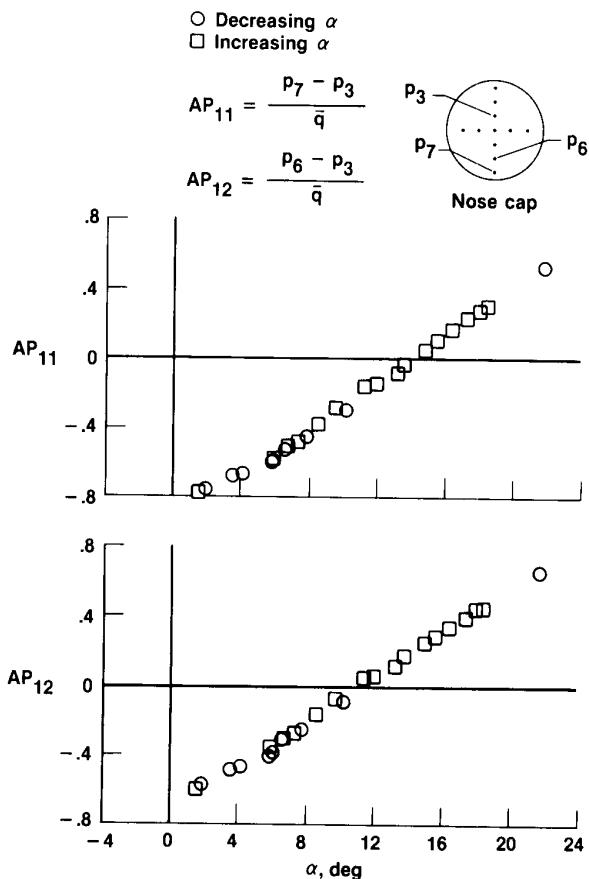
(d) *M = 0.90, orifices on nose cap.*
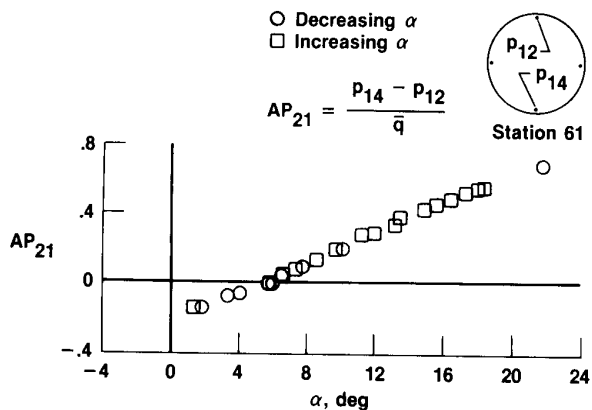
(e) *M = 0.90, orifices at station 61.*
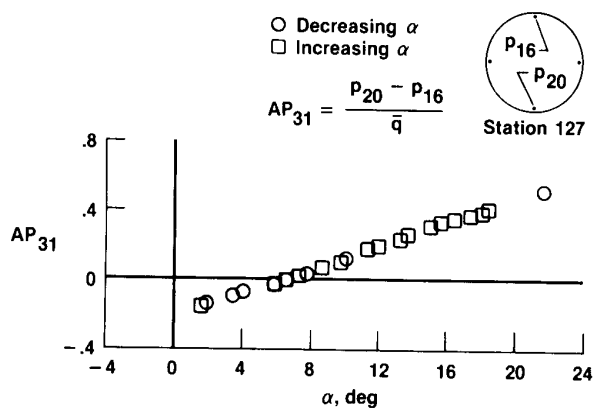
(f) *M = 0.90, orifices at station 127.*

Figure 20. Continued.

48
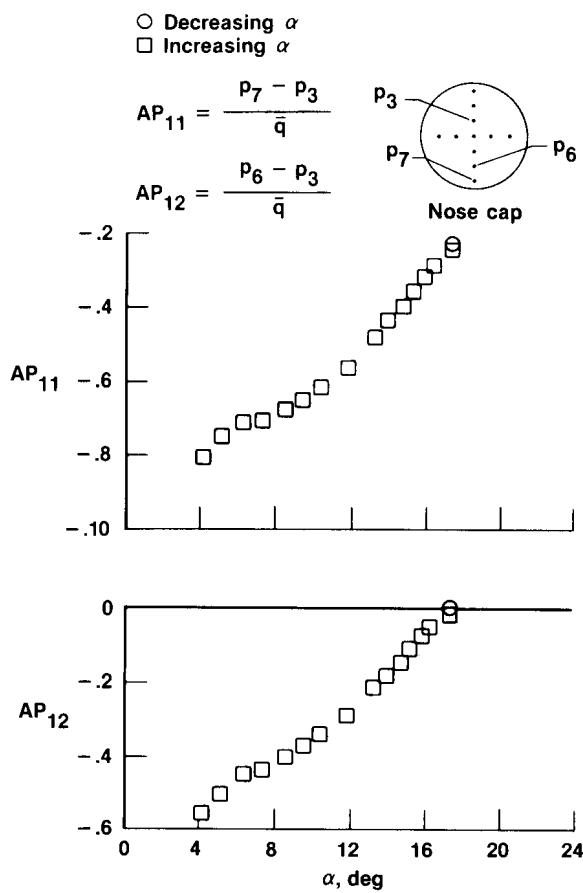
(g) M = 1.23, orifices on nose cap.
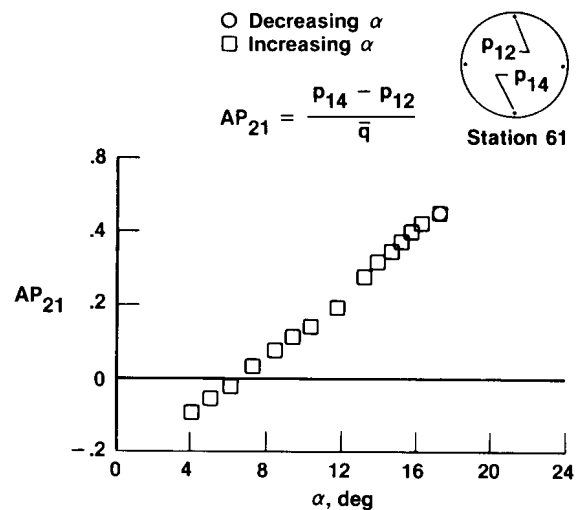
(h) M = 1.23, orifices at station 61.
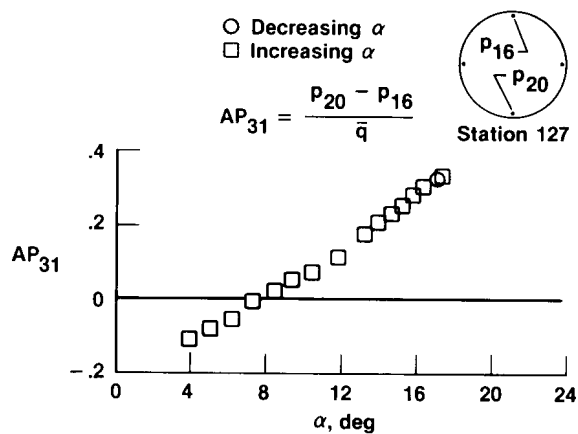
(i) M = 1.23, orifices at station 127.

Figure 20. Concluded.

O Decreasing α
□ Increasing α

$$AP_{11} = \frac{p_7 - p_3}{\bar{q}}$$

$$AP_{12} = \frac{p_6 - p_3}{\bar{q}}$$

$$AP_{21} = \frac{p_{14} - p_{12}}{\bar{q}}$$

$$AP_{31} = \frac{p_{20} - p_{16}}{\bar{q}}$$
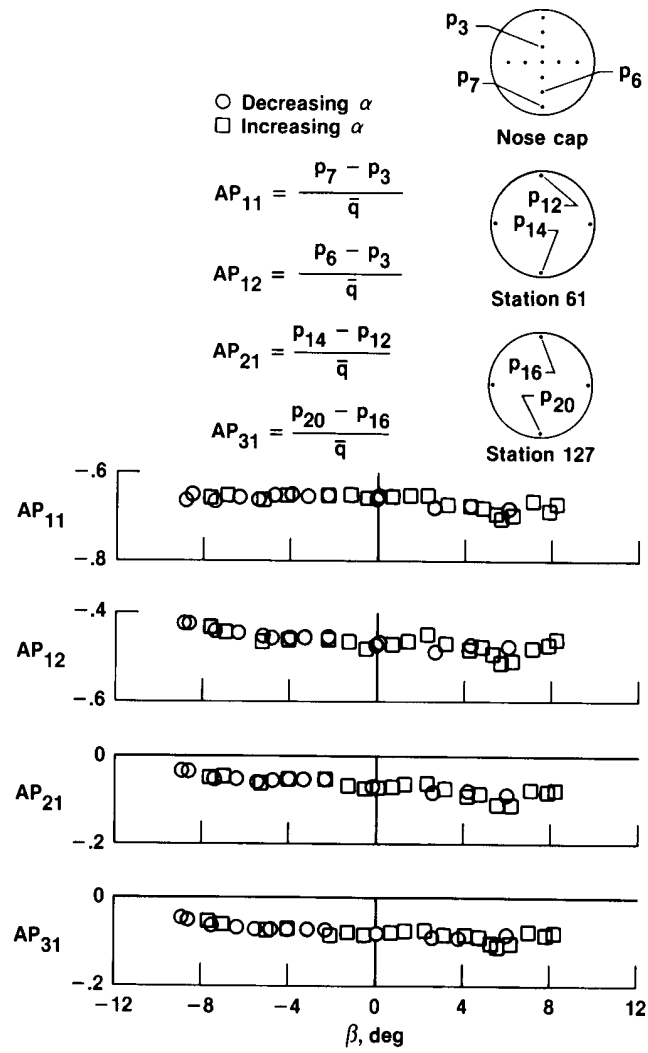
Figure 21. Effect of sideslip on angle-of-attack parameter, $M = 0.90$ and $\alpha = 4.0°$.

$$AP_{11} = \frac{p_7 - p_3}{\bar{q}}$$

$$AP_{12} = \frac{p_6 - p_3}{\bar{q}}$$

$$AP_{21} = \frac{p_{14} - p_{12}}{\bar{q}}$$

$$AP_{31} = \frac{p_{20} - p_{16}}{\bar{q}}$$

(a) α = 0°.
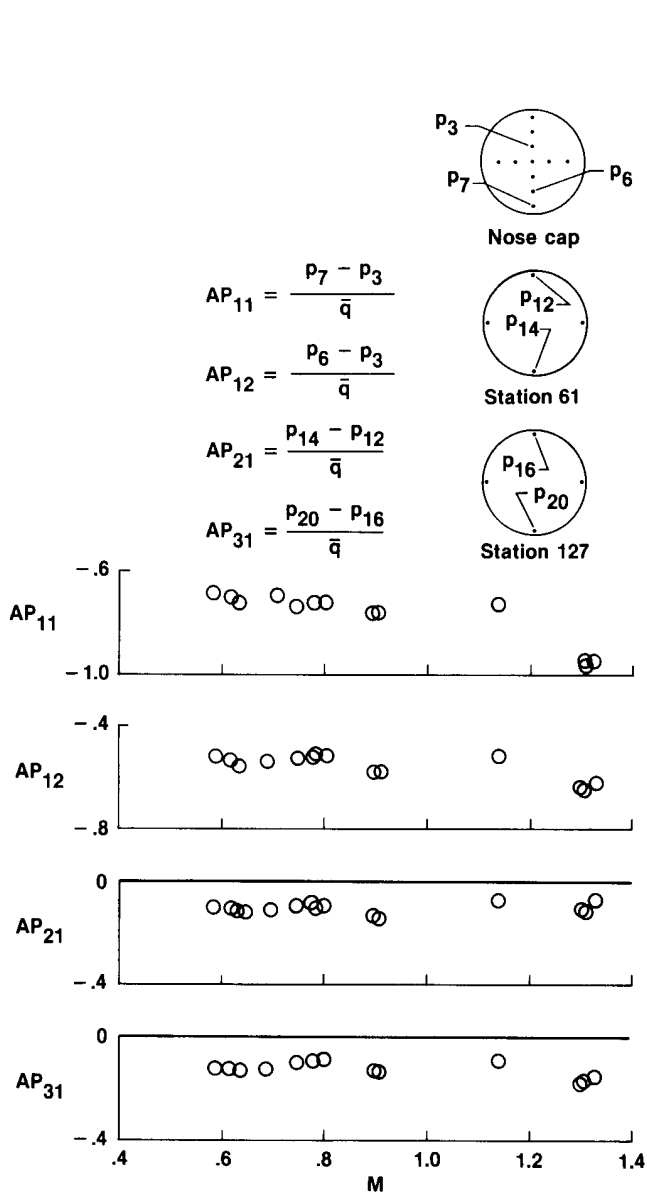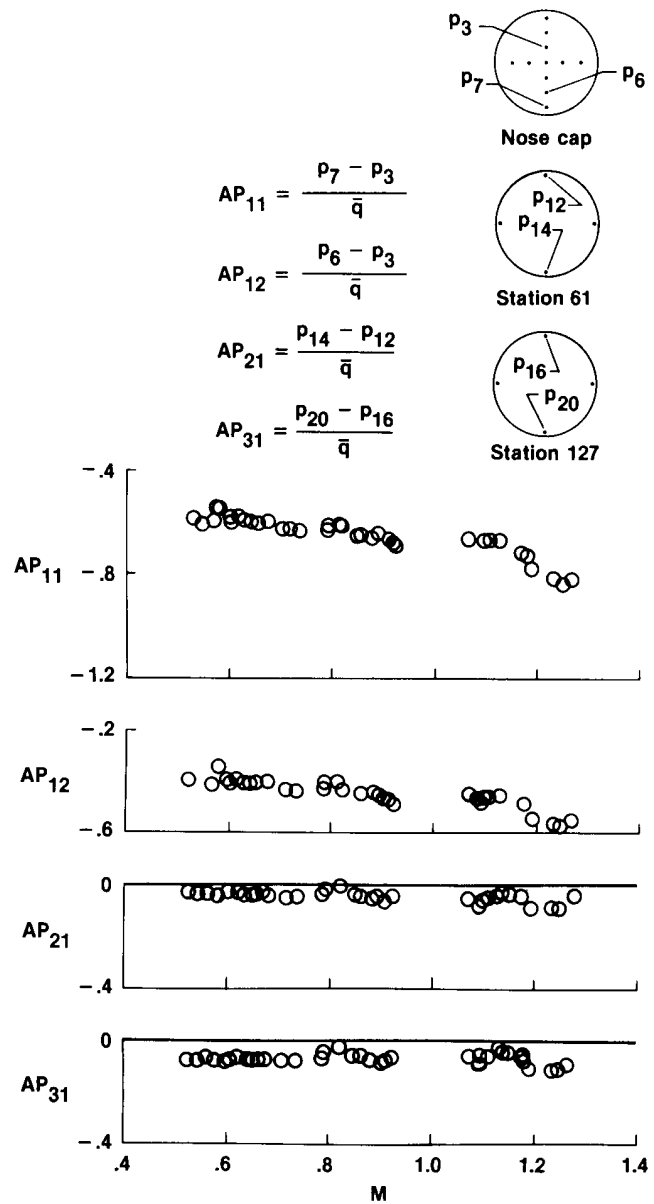
(b) α = 4.0°.

Figure 22. Effect of Mach on angle-of-attack parameter.

51

$$AP_{11} = \frac{p_7 - p_3}{\bar{q}}$$

$$AP_{12} = \frac{p_6 - p_3}{\bar{q}}$$

$$AP_{21} = \frac{p_{14} - p_{12}}{\bar{q}}$$

$$AP_{31} = \frac{p_{20} - p_{16}}{\bar{q}}$$
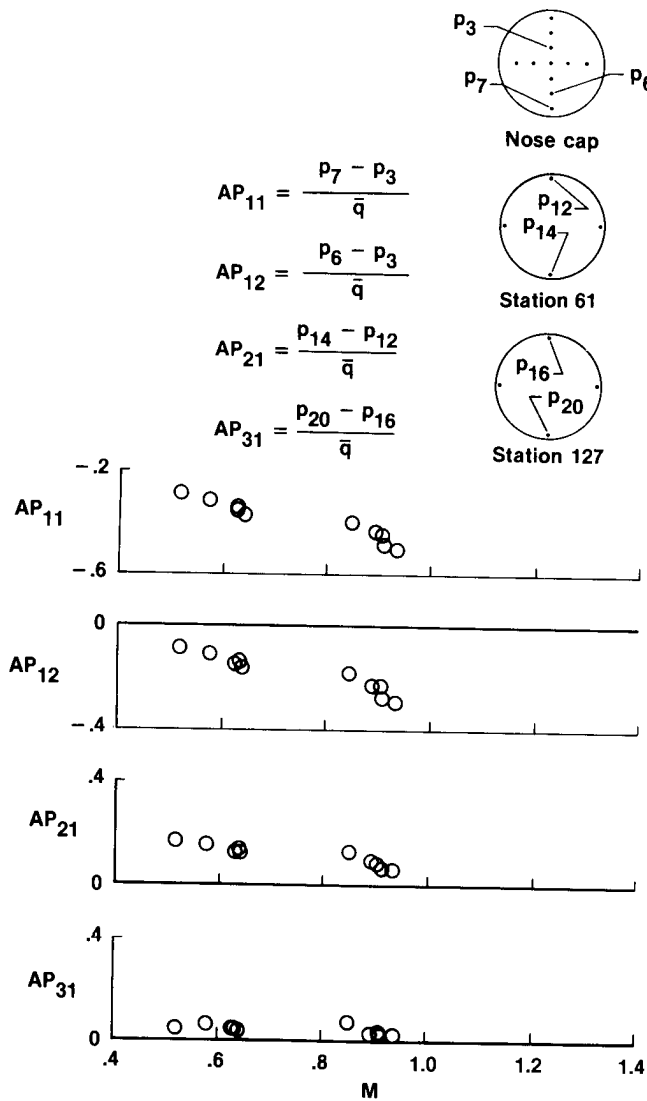
(c) $\alpha = 8.0°$.

Figure 22. Concluded.
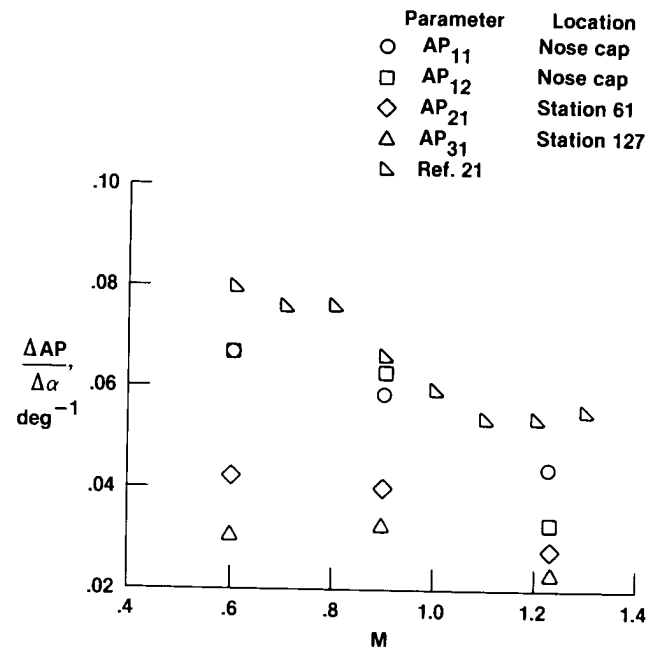
Figure 23. Angle-of-attack sensitivity factor as a function of Mach.
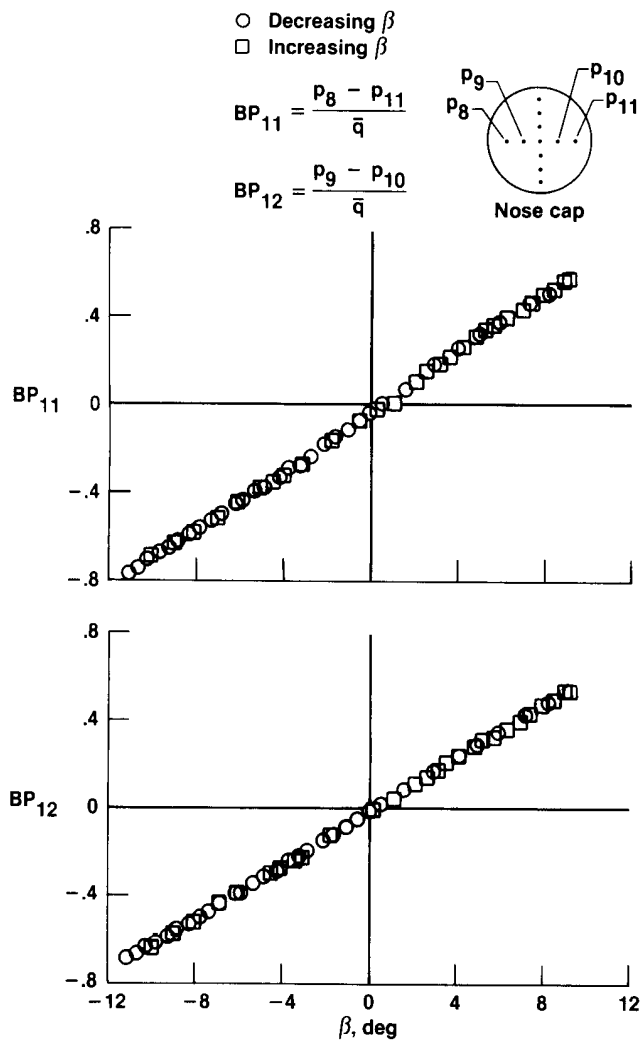
(a) $M = 0.77$, $\alpha = 1.9°$ to $3.6°$, orifices on nose cap.
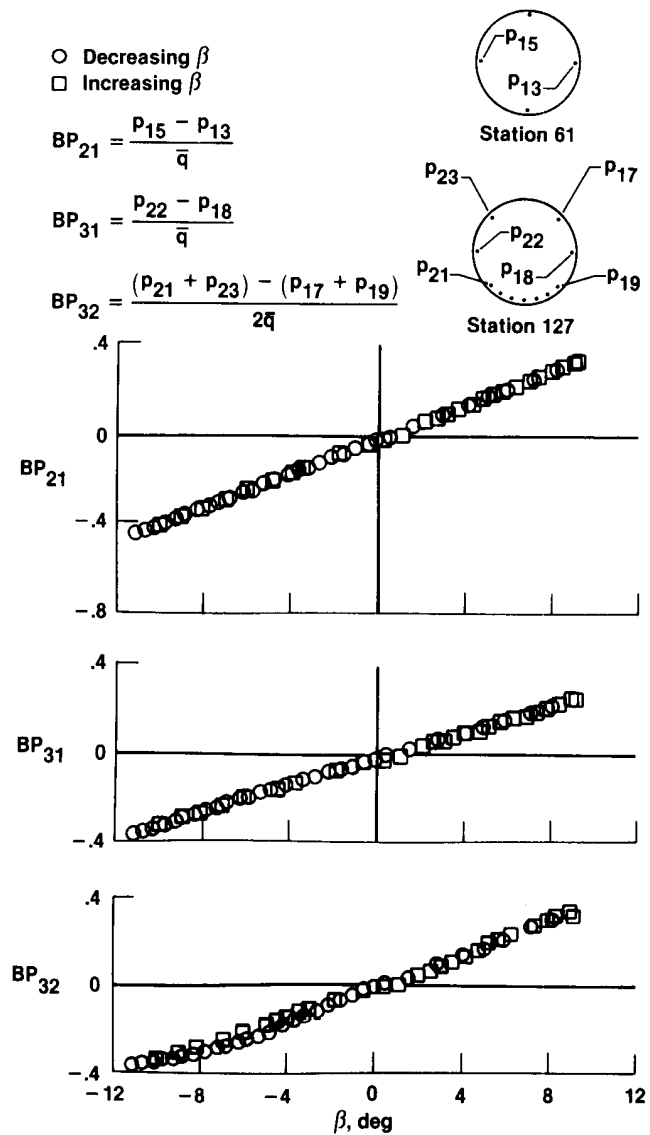
(b) $M = 0.77$, $\alpha = 1.9°$ to $3.6°$, orifices at stations 61 and 127.

Figure 24. Angle-of-sideslip parameter as a function of angle of sideslip.
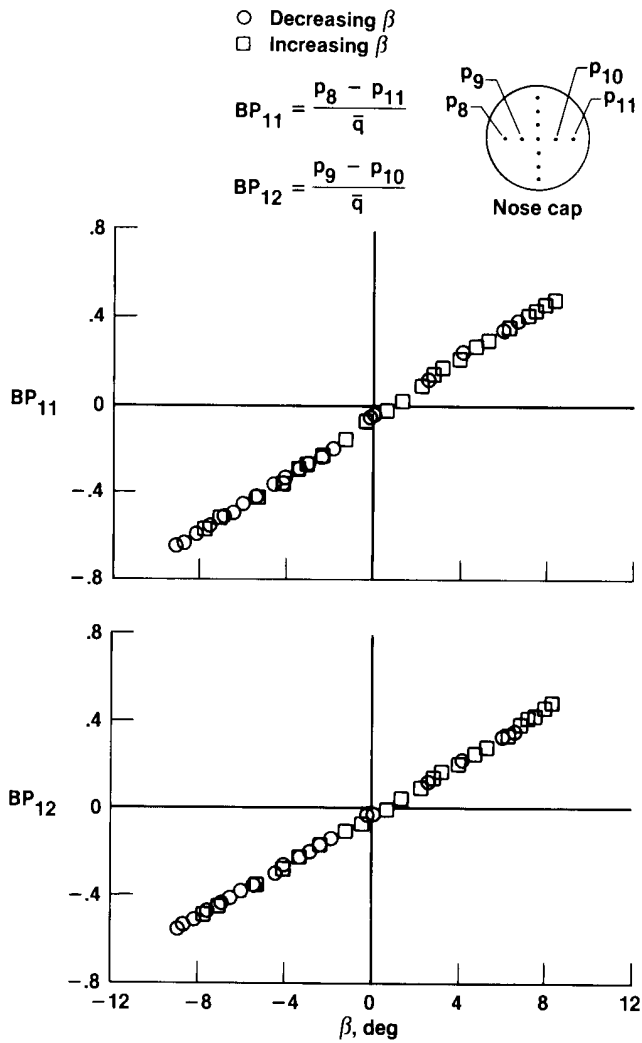
(c) M = 0.89, α = 3.3° to 5.6°, orifices on nose cap.
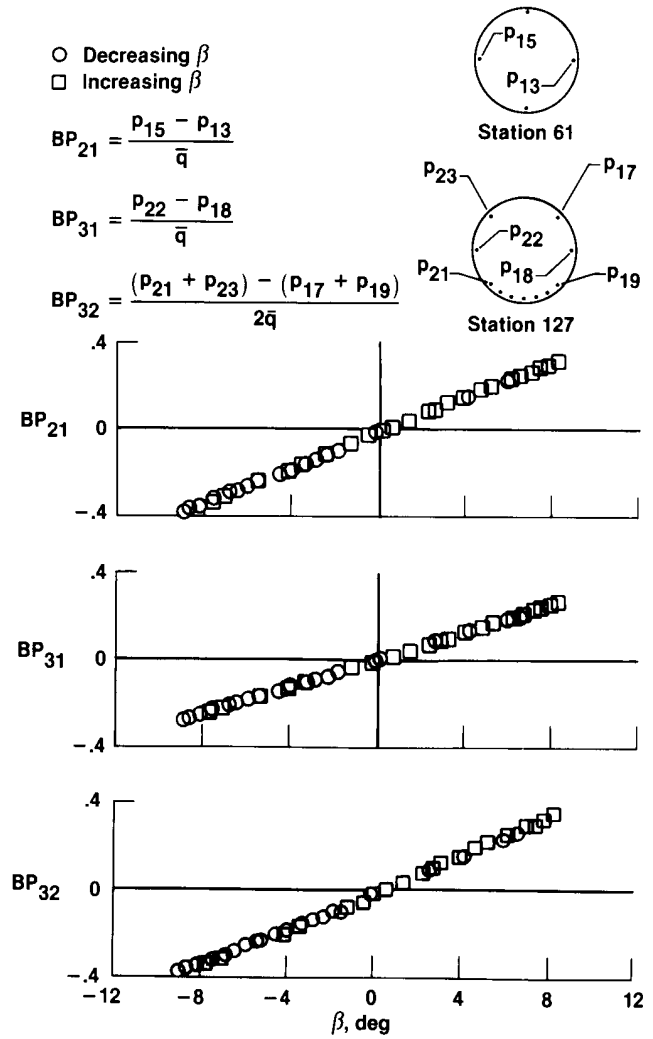
(d) M = 0.89, α = 3.3° to 5.6°, orifices at stations 61 and 127.

Figure 24. Concluded.
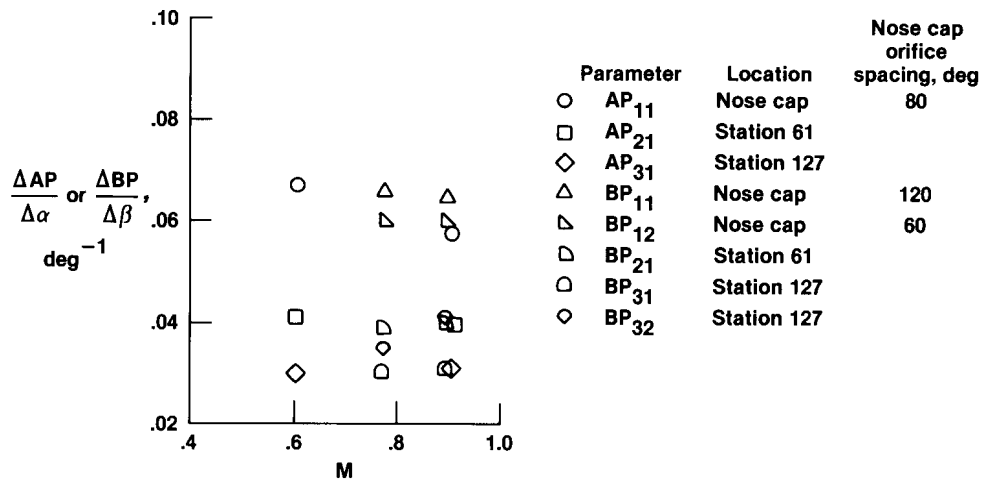
Figure 25. Sensitivity factor for angle of attack or angle of sideslip as a function of Mach.

(a) p_3/p_6.
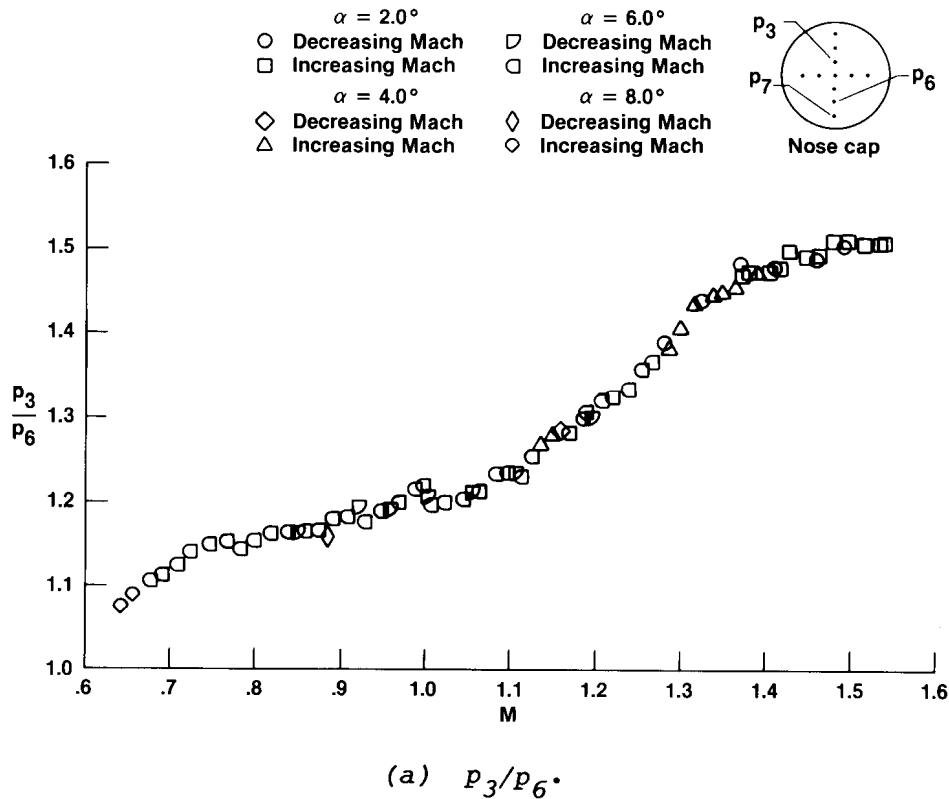
Figure 26. Pressure ratio for determining Mach using nose cap orifices only.
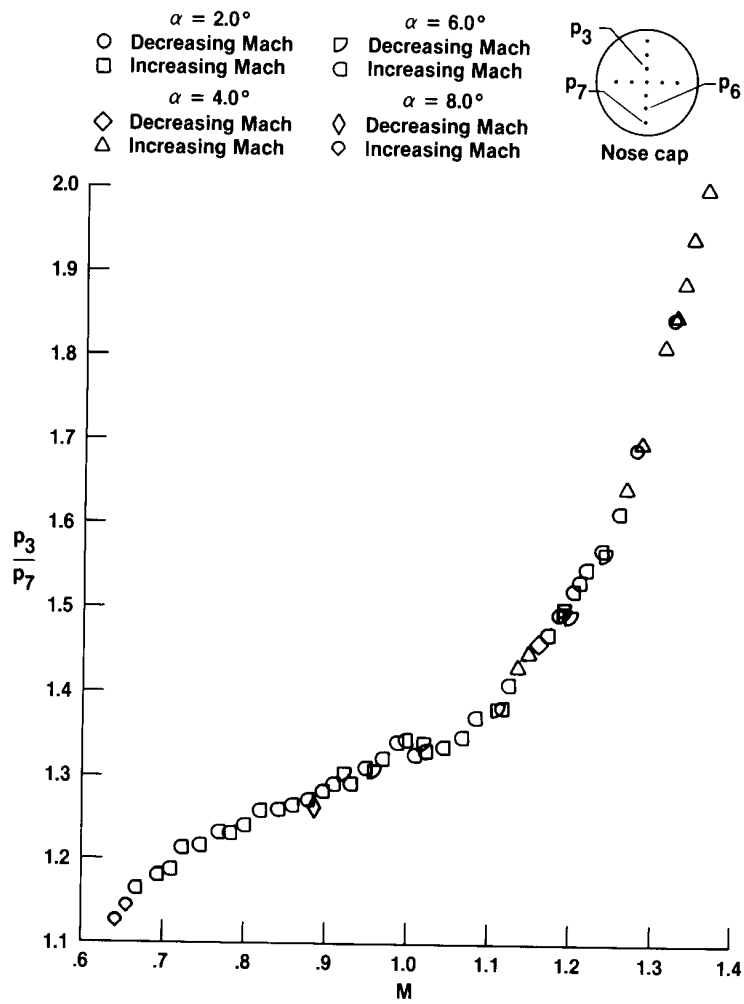
(b) p_3/p_7.

Figure 26. Concluded.
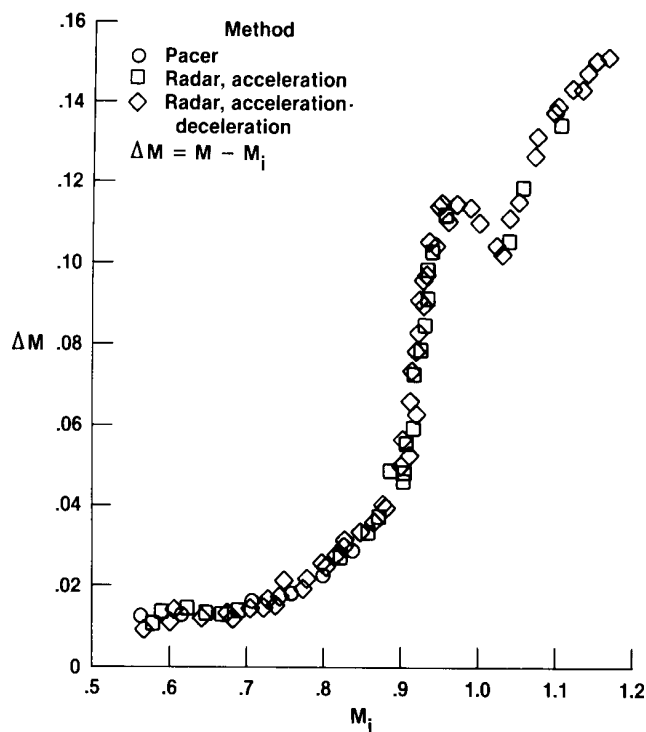
Figure 27. Typical results of Mach correction for static-pressure position error of IR reference probe as a function of indicated Mach, α = 1.7° to 2.7°.
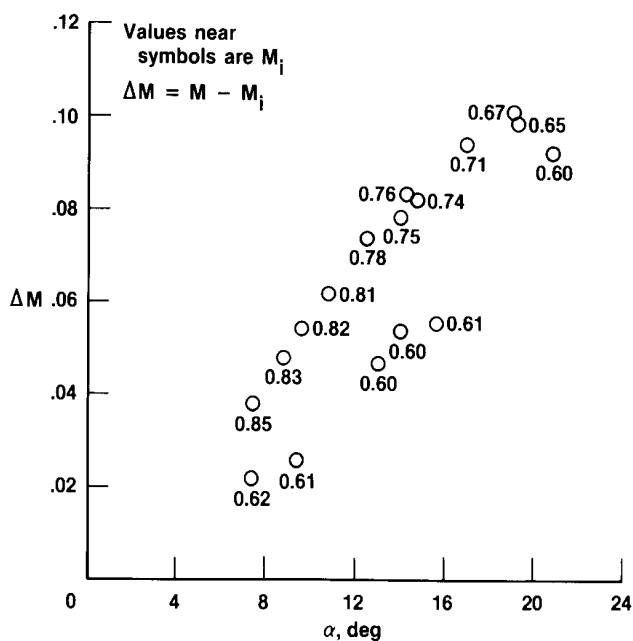
Figure 28. Mach correction for static-pressure position error of IR reference probe as a function of angle of attack for different indicated Mach numbers.
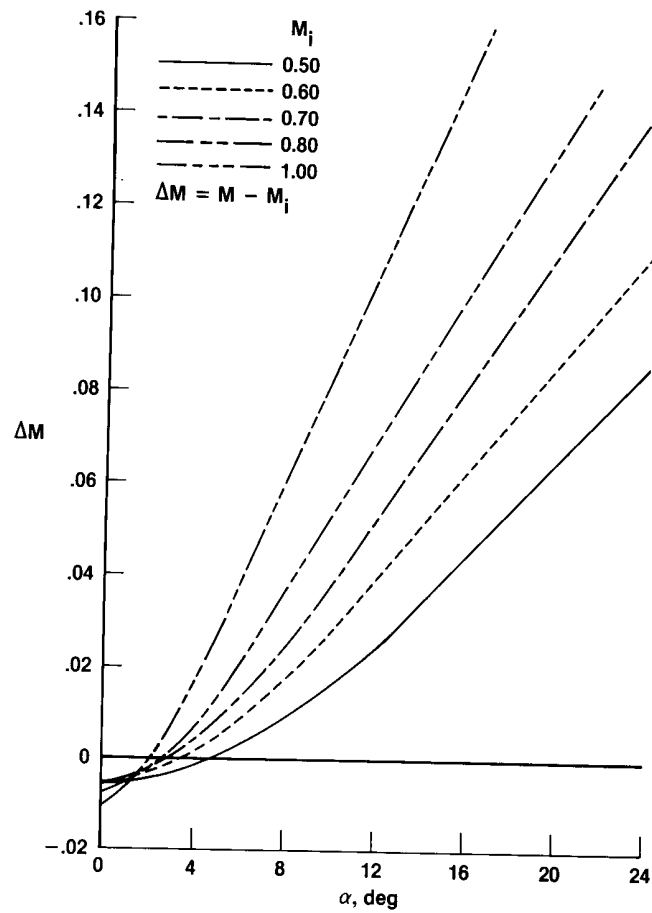
Figure 29. Mach correction for static-pressure position error of IR reference probe as a function of angle of attack at constant indicated Mach.
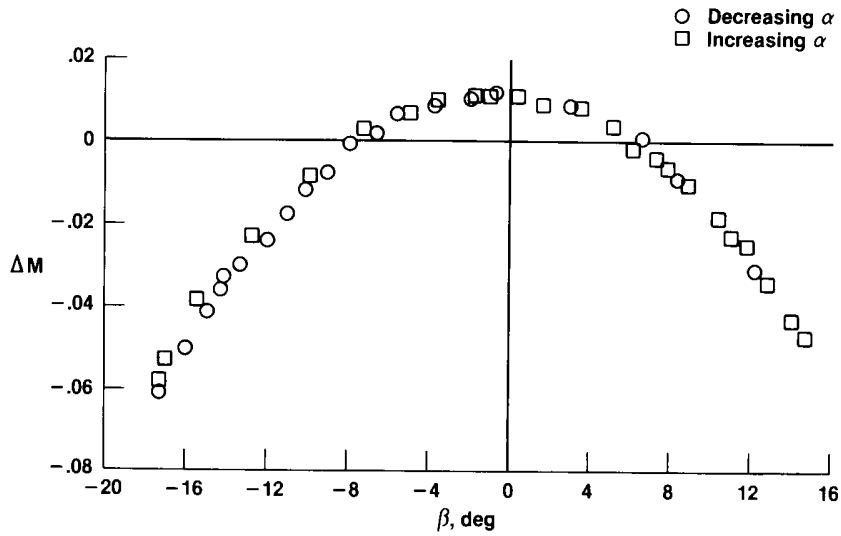
Figure 30. Mach correction for static-pressure position error of IR reference probe as a function of angle of sideslip, M = 0.60 and α ≈ 5.0°.

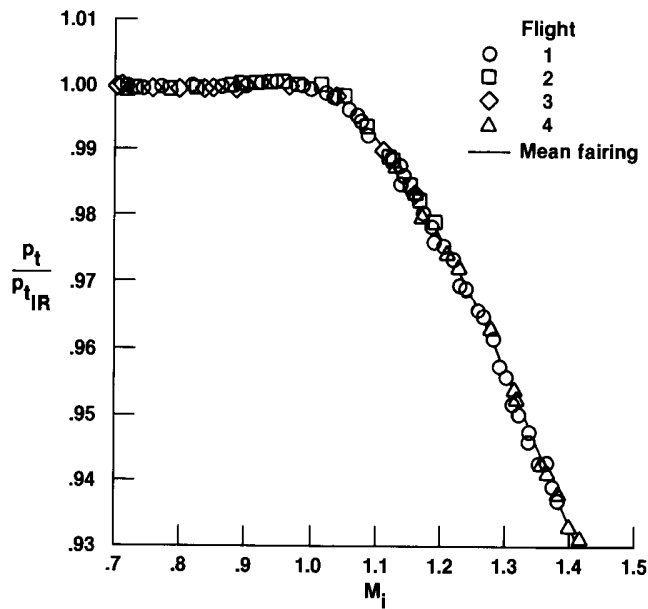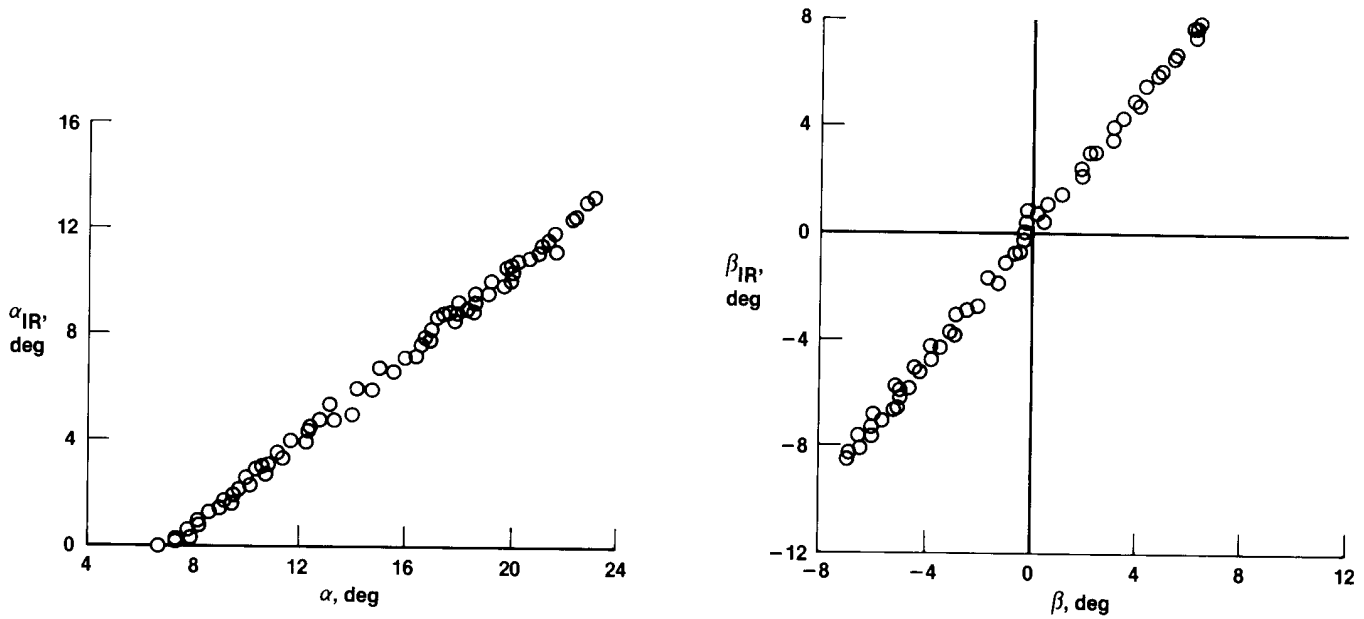
Figure 31. Ratio of stagnation pressure of nose boom to stagnation pressure of IR reference probe as a function of indicated Mach, α < 10.0°.

(a)   Angle of attack, M_i = 0.53 to 0.63.

(b)   Angle of sideslip, M_i = 0.86 to 0.88.

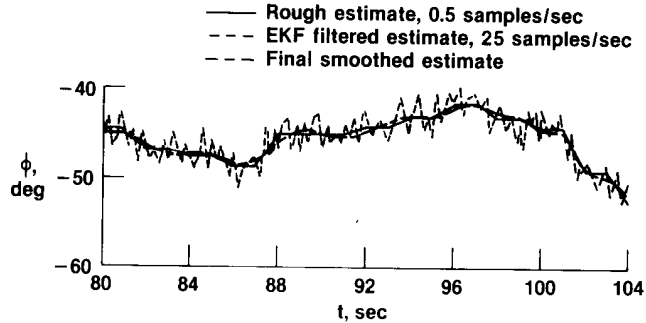Figure 32.   Angle-of-attack and angle-of-sideslip calibration data.

Figure 33.   Typical time history of reconstructed roll angles, including rough, filtered, and smoothed estimates.
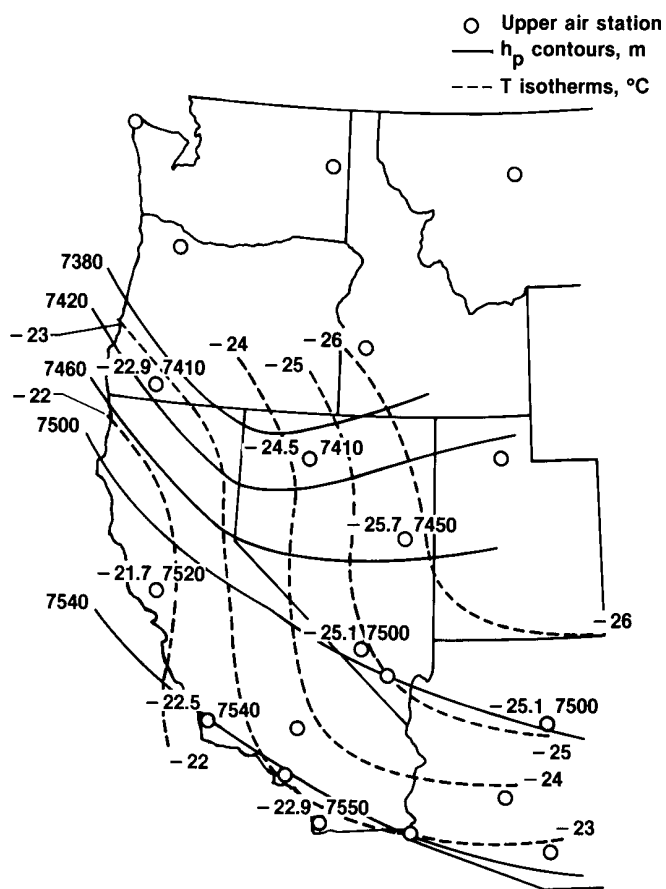
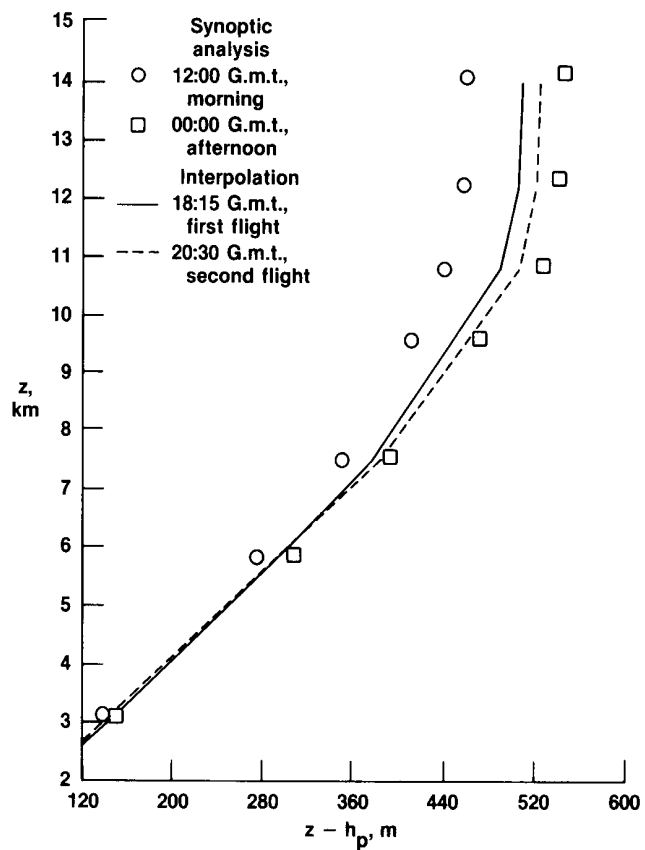*Figure 34. Synoptic meteorological analysis for 400-mbar surface, h_p = 7.19 km.*

Figure 35. Geometric altitude profile of difference between geometric altitude and pressure altitude.

1. Report No. NASA TP-2716	2. Government Accession No.	3. Recipient's Catalog No.
4. Title and Subtitle Qualitative Evaluation of a Flush Air Data System at Transonic Speeds and High Angles of Attack		5. Report Date April 1987
		6. Performing Organization Code
7. Author(s) Terry J. Larson, Stephen A. Whitmore, L. J. Ehernberger, J. Blair Johnson, and Paul M. Siemers III		8. Performing Organization Report No. H-1277
		10. Work Unit No. RTOP 505-68-31
9. Performing Organization Name and Address NASA Ames Research Center Dryden Flight Research Facility P.O. Box 273 Edwards, CA 93523-5000		
		11. Contract or Grant No.
		13. Type of Report and Period Covered Technical Paper
12. Sponsoring Agency Name and Address National Aeronautics and Space Administration Washington, DC 20546		
		14. Sponsoring Agency Code

15. Supplementary Notes

Mssrs. Larson, Whitmore, Ehernberger, and Johnson are affiliated with Ames-Dryden Flight Research Facility; Mr. Siemers is affiliated with Langley Research Center.

16. Abstract

Flight tests were performed on an F-14 aircraft to evaluate the use of flush pressure orifices on the nose section for obtaining air data at transonic speeds over a large range of flow angles. This program, conducted at the Dryden Flight Research Facility of NASA Ames Research Center, was part of a flight test and wind-tunnel program to assess the accuracies of such systems for general use on aircraft. It also provided data to validate algorithms developed for the shuttle entry air data system designed at NASA Langley Research Center. Data were obtained for Mach numbers between 0.60 and 1.60, for angles of attack up to 26.0°, and for sideslip angles up to 11.0°. With careful calibration, a flush air data system with all flush orifices can provide accurate air data information over a large range of flow angles. Several orifices on the nose cap were found to be suitable for determination of stagnation pressure. Other orifices on the nose section aft of the nose cap were shown to be suitable for determination of static pressure. Pairs of orifices on the nose cap provided the most sensitive measurements for determining angles of attack and sideslip, although orifices located farther aft on the nose section could also be used.

17. Key Words (Suggested by Author(s)) Air data Flow-angle measurements Flush air data system Flush pressure orifice measurements Pitot-static measurements	18. Distribution Statement Unclassified — Unlimited Subject Category 05
19. Security Classif. (of this report) Unclassified	20. Security Classif. (of this page) Unclassified	21. No. of Pages 62	22. Price* A04